Comput. Methods Appl. Mech. Engrg. 197 (2008) 3883–3897

Contents lists available at ScienceDirect

Comput. Methods Appl. Mech. Engrg.

journal homepage: www.elsevier.com/locate/cma

A novel alpha finite element method (αFEM) for exact solution to mechanics problems using triangular and tetrahedral elements

G.R. Liu [a,b], T. Nguyen-Thoi [a,*], K.Y. Lam [c]

[a] Center for Advanced Computations in Engineering Science (ACES), Department of Mechanical Engineering, National University of Singapore, 9 Engineering Drive 1, Singapore 117576, Singapore
[b] Singapore-MIT Alliance (SMA), E4-04-10, 4 Engineering Drive 3, Singapore 117576, Singapore
[c] School of Mechanical and Aerospace Engineering, Nanyang Technological University, 50 Nanyang Avenue, Singapore 639798, Singapore

ARTICLE INFO

Article history:
Received 3 November 2007
Received in revised form 3 March 2008
Accepted 11 March 2008
Available online 27 March 2008

Keywords:
Numerical methods
Finite element method (FEM)
Node-based smoothed finite element method (N-SFEM)
Upper bound
Lower bound
Alpha finite element method (αFEM)

ABSTRACT

The paper presents an alpha finite element method (αFEM) for computing nearly exact solution in energy norm for mechanics problems using meshes that can be generated automatically for arbitrarily complicated domains. Three-node triangular (αFEM-T3) and four-node tetrahedral (αFEM-T4) elements with a scale factor α are formulated for two-dimensional (2D) and three-dimensional (3D) problems, respectively. The essential idea of the method is the use of a scale factor $\alpha \in [0,1]$ to obtain a combined model of the standard fully compatible model of the FEM and a quasi-equilibrium model of the node-based smoothed FEM (N-SFEM). This novel combination of the FEM and N-SFEM makes the best use of the upper bound property of the N-SFEM and the lower bound property of the standard FEM. Using meshes with the same aspect ratio, a unified approach has been proposed to obtain a nearly exact solution in strain energy for linear problems. The proposed elements are also applied to improve the accuracy of the solution of nonlinear problems of large deformation. Numerical results for 2D (using αFEM-T3) and 3D (using αFEM-T4) problems confirm that the present method gives the much more accurate solution comparing to both the standard FEM and the N-SFEM with the same number of degrees of freedom and similar computational efforts for both linear and nonlinear problems.

1. Introduction

For many decades, the constant finite elements such as the three-node triangle and four-node tetrahedron are popular and widely used in practical. The reason is that these elements can be easily formulated and implemented very effectively in the finite element programs using piecewise linear approximation. Furthermore, most FEM (finite element method) codes for adaptive analyses are based on triangular and tetrahedral elements, due to the simple fact that triangular and tetrahedral meshes can be automatically generated.

However, these elements possess significant shortcomings, such as poor accuracy in stress solution, the overly stiff behavior and volumetric locking for plane strain problems in the nearly incompressible cases. In order to overcome these disadvantages, some new finite elements were proposed. For the triangular elements, Allman [1,2] introduced rotational degrees of freedom at the element nodes to achieve an improvement for the overly stiff behavior. Elements with rotational degrees of freedom were also considered in Ref. [3,4]. Piltner and Taylor [5] combined the rotational degrees of freedom and enhanced strain modes to give a triangular element which can achieve a higher convergence in energy and deal with the nearly incompressible plane strain problems. However, using more degrees of freedom at the nodes limits the practical application of those methods. For both triangular and tetrahedral elements, Dohrmann et al. [6] presented a weighted least-squares approach in which a linear displacement field is fit to an element's nodal displacements. The method is claimed to be computationally efficient and avoids the volumetric locking problems. However, more nodes are required on the element boundary to define the linear displacement field. Dohrmann et al. [7] also proposed a nodal integration finite element method (NI-FEM) in which each element is associated with a single node and the linear interpolation functions of the original mesh are used. The method avoids the volumetric locking problems and performs better comparing to standard triangular and tetrahedral elements in terms of stress solution for static problems.

In the other front of development, a conforming nodal integration technique has been proposed by Chen et al. [8] to stabilize the solutions in the context of the meshfree method and then applied in the natural-element method [9]. Liu et al. have applied this technique to formulate the linear conforming point interpolation method (LC-PIM) [10], the linearly conforming radial point

* Corresponding author. Tel.: +65 9860 4962.
E-mail address: g0500347@nus.edu.sg (T. Nguyen-Thoi).

0045-7825/$ - see front matter © 2008 Elsevier B.V. All rights reserved.
doi:10.1016/j.cma.2008.03.011

interpolation method (LC-RPIM) [11]. Applying the same idea to the FEM, an element-based smoothed finite element method (SFEM) [12,13,43] and a node-based smoothed finite element method (N-SFEM) [14] have also been formulated. When only the linear shape function for interpolation is used, the LC-PIM is identical to the NI-FEM or N-SFEM using triangular and tetrahedral elements [14]. Liu et al. [15] have provided an intuitive explanation and showed numerically that when a reasonably fine mesh is used, the LC-PIM has an upper bound in the strain energy. The same finding is obtained for LC-RPIM and N-SFEM, meaning that the LC-RPIM and N-SFEM also have the similar upper bound property.

Obtaining exact solution measured in a norm using a numerical method is a fascinating idea in the area of computational methods. So far, the mixed FEM models [16–19] based on the mixed variational principles focus mainly to improve the accuracy of the solution. Recently, an alpha finite element method (αFEM) using four-node quadrilateral elements has been developed for the purpose of finding the nearly exact solution in strain energy even for the coarse mesh [20,21]. The αFEM is a novel FEM in which the gradient of strains is scaled by a factor $\alpha \in [0,1]$, and the coding of the αFEM is almost exactly the same as the standard FEM. The obtained result of strain energy is a continuous function of α between the solutions of the standard FEM using reduced integration and that using full Gauss integration. The significance of this formulating is two folds: (1) For overestimation problems, there exists an $\alpha \in [0,1]$ at which the solutions of αFEM is nearly exact in energy norm; (2) For underestimation problems, the αFEM solution obtained at $\alpha = 0$ is the closest to the exact solution in energy norm [20,21]. Based on the function of strain energy curves and the use of meshes with the same aspect ratio, a general procedure of the αFEM has been suggested to obtain the exact or best possible solution for a given problem: an exact-α approach is devised for overestimation problems; and a zero-α approach for underestimation problems. The αFEM has clearly opened a novel window of opportunity to obtain numerical solutions that are exact in certain norms. However, the αFEM based on quadrilateral elements cannot provide exact solution to all problems. Furthermore, the use of four-node quadrilateral elements in αFEM requires a quadrilateral mesh that cannot be generated in a full automated manner for complicated domains.

Making use of the upper bound property of the N-SFEM, the lower bound property of the standard FEM in the strain energy, and the importance idea of the αFEM for the four-node quadrilateral elements, we propose a novel alpha finite element method using three-node triangular (αFEM-T3) elements for 2D problems and four-node tetrahedral elements (αFEM-T4) for 3D problems. The essential idea of the method is to introduce a scale factor $\alpha \in [0,1]$ to establish a continuous function of strain energy that contains contributions from both the standard FEM and the N-SFEM. Our formulation ensures the variational consistence and the compatibility of the displacement field, and hence guarantees reproducing linear field exactly. Based on the fact that the standard FEM of triangular and tetrahedral elements is stable (no spurious zero energy modes), and so is the N-SFEM as proved by Liu et al. [14], our αFEM will be always stable. This stability ensures the convergence of the solution. Furthermore, this novel combined formulation of the FEM and N-SFEM makes the best use of the upper bound property of the N-SFEM and the lower bound property of the standard FEM. Using meshes with the same aspect ratio, a unified approach has been proposed to obtain the nearly exact solution in strain energy for a given linear problem. The proposed elements are also applied to nonlinear problems of large deformation. In such cases, the exact solution is usually difficult to obtain, but the accuracy of the solution can be significantly improved. Numerical results for 2D (using αFEM-T3) and 3D (using αFEM-T4) problems confirm that the present method gives the excellent performance comparing to both the standard FEM and the N-SFEM. It is very easy to implement and apply to practical problems of complicated geometry.

Note that the present αFEM-T3 and αFEM-T4 are very much different from the αFEM for quadrilateral elements (or αFEM-Q4) given in Ref. [20,21] in terms of both formulation procedures and the approach. First, the αFEM-Q4 is element based and αFEM-T3 (or αFEM-T4) is both element and node based; Second, in the case of αFEM-Q4, the strain field in the element is linear, which allows us to scale the gradient of the strain field by introducing a scaling factor α. In the present αFEM-T3 (or αFEM-T4), the strain field in the element is constant, and hence it is not possible to scale the gradient of the strain field. Therefore, a new technique has to be devised to create a desirable strain field; Third, αFEM-Q4 can only give nearly exact solution in strain energy for overestimation problems [20,21], while the present αFEM-T3 (or αFEM-T4) can provide nearly exact solution in strain energy for all linear problems without any post processing techniques.

The paper is outlined as follows. In Section 2, the idea the αFEM-T3 and αFEM-T4 is briefly introduced. In Section 3, some theoretical properties of the αFEM-T3 and αFEM-T4 are presented. Numerical implementations are described in Section 4 and patch testes are performed in Section 5. In Section 6, some numerical examples are examined and discussed to verify the formulations and properties of the αFEM-T3 and αFEM-T4. Some concluding remarks are made in the Section 7.

2. The idea of the present αFEM

2.1. Briefing on the finite element method (FEM) [22–26]

The discrete equations of the FEM are generated from the Galerkin weak form

$$\int_\Omega (\nabla_s \delta\mathbf{u})^{\mathrm{T}} \mathbf{D} (\nabla_s \mathbf{u})\, \mathrm{d}\Omega - \int_\Omega \delta\mathbf{u}^{\mathrm{T}} \mathbf{b}\, \mathrm{d}\Omega - \int_{\Gamma_t} \delta\mathbf{u}^{\mathrm{T}} \bar{\mathbf{t}}\, \mathrm{d}\Gamma = 0, \tag{1}$$

where $\mathbf{b}$ is the vector of external body forces, $\mathbf{D}$ is a symmetric positive definite (SPD) matrix of material constants, $\bar{\mathbf{t}}$ is the prescribed traction vector on the natural boundary Γ_t, $\mathbf{u}$ is trial functions, $\delta\mathbf{u}$ is test functions and $\nabla_s\mathbf{u}$ is the symmetric gradient of the displacement field.

The FEM uses the following trial and test functions

$$\mathbf{u}^h(\mathbf{x}) = \sum_{I=1}^{\mathrm{NP}} \mathbf{N}_I(\mathbf{x})\mathbf{d}_I; \quad \delta\mathbf{u}^h(\mathbf{x}) = \sum_{I=1}^{\mathrm{NP}} \mathbf{N}_I(\mathbf{x})\delta\mathbf{d}_I, \tag{2}$$

where NP is the number of the nodal variables of the element, $\mathbf{d}_I$ is the nodal displacement vector, and $\mathbf{N}_I(\mathbf{x})$ is a matrix of shape functions.

By substituting the approximations, $\mathbf{u}^h$ and $\delta\mathbf{u}^h$, into the weak form and invoking the arbitrariness of virtual nodal displacements, Eq. (1) yields the standard discretized algebraic equation system:

$$\mathbf{K}^{\mathrm{FEM}}\mathbf{d} = \mathbf{f}, \tag{3}$$

where $\mathbf{K}^{\mathrm{FEM}}$ is the system stiffness matrix, $\mathbf{f}$ is the force vector, that are assembled with entries of

$$\mathbf{K}_{IJ}^{\mathrm{FEM}} = \int_{\Omega_e} \mathbf{B}_I^{\mathrm{T}} \mathbf{D} \mathbf{B}_J\, \mathrm{d}\Omega, \tag{4}$$

$$\mathbf{f}_I = \int_{\Omega_e} \mathbf{N}_I^{\mathrm{T}}(\mathbf{x})\mathbf{b}\, \mathrm{d}\Omega + \int_{\Gamma_t} \mathbf{N}_I^{\mathrm{T}}(\mathbf{x})\bar{\mathbf{t}}\, \mathrm{d}\Gamma. \tag{5}$$

In Eq. (4), the *strain matrix* is defined as

$$\mathbf{B}_I(\mathbf{x}) = \nabla_s N_I(\mathbf{x}) \tag{6}$$

that produces *compatible* strain fields. Using the triangular and tetrahedral elements with the linear shape functions, the strain

gradient matrix $\mathbf{B}_I(\mathbf{x})$ contains only constant entries. Eq. (4) then becomes

$$\mathbf{K}_{IJ}^{\mathrm{FEM}} = \mathbf{B}_I^{\mathrm{T}}\mathbf{D}\mathbf{B}_J V_e, \tag{7}$$

where $V_e = \int_{\Omega_e} \mathrm{d}\Omega$ is the area/volume of the element.

2.2. Briefing on node-based smoothed finite element method (N-SFEM)

The N-SFEM works for polygonal elements of arbitrary sides [14]. Here we brief only the formulations for triangular element N-SFEM-T3 for 2D problems and the tetrahedral element N-SFEM-T4 for 3D problems, because they will be used in this work.

In the N-SFEM-T3 for 2D problems, the domain discretization is the same as that of the standard FEM using N_e triangular elements, but the integration required in the weak form (1) is performed based on the nodes, and strain smoothing technique [8] is used. In such a nodal integration process, the problem domain Ω is divided into smoothing cells associated with nodes such that $\Omega = \Omega^{(1)} \cup \Omega^{(2)} \cup \cdots \cup \Omega^{(N_n)}$ and $\Omega^{(i)} \cap \Omega^{(j)} = \emptyset$, $i \neq j$, in which N_n is the number of total nodes located in the entire problem domain. For triangular elements, the cell $\Omega^{(k)}$ associated with the node k is created by connecting sequentially the mid-edge-points to the centroids of the surrounding triangular elements of the node k as shown in Fig. 1. As a result, each triangular element will be divided into three quadrilaterals of equal area and each quadrilateral is attached with the nearest node. The cell $\Omega^{(k)}$ associated with the node k is then created by combination of each nearest quadrilateral of all elements surrounding the node k.

Similarly in the N-SFEM-T4 for 3D problems, each tetrahedral element will be divided into four sub-domains of equal area and each sub-domain is attached with the nearest node. Combine each sub-domain of all elements surrounding the node k forms the cell $\Omega^{(k)}$ associated with the node k. The formulation of the N-SFEM-T4 is very much the same as the N-SFEM-T3, and hence our discussion will focus on N-SFEM-T3.

In the N-SFEM [14], the domain integration over the smoothing cell $\Omega^{(k)}$ for computing the smoothed strain gradient matrix $\widetilde{\mathbf{B}}$ becomes line integrations along the boundary $\Gamma^{(k)}$ of the cell. The gradients are computed directly only using shape functions itself at some particular points along segments of boundary of the cells and no explicit analytical form is required. The values of shape functions at any point in an n-sided polygonal element are defined in a trivial manner of simple interpolation [14].

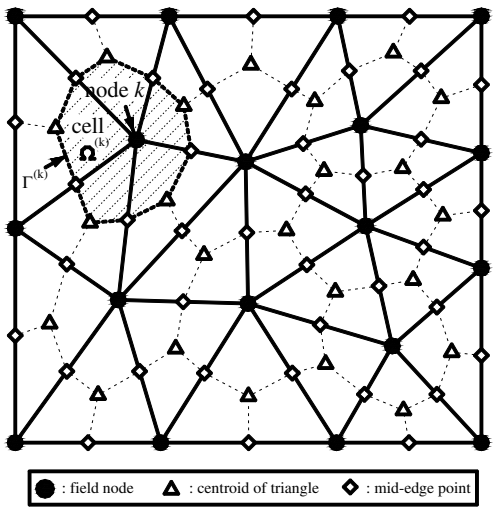

Fig. 1. Triangular elements and smoothing cells associated with the nodes.

In this paper, however, due to the use the standard FEM together the N-SFEM in the αFEM-T3 and αFEM-T4, the formulation of N-SFEM will be performed in an alternative way. This change aims to reuse the stiffness gradient matrix $\mathbf{B}_I$ of the elements in the standard FEM to calculate the smoothed stiffness gradient matrix $\widetilde{\mathbf{B}}_I(\mathbf{x}_k)$ of the cell $\Omega^{(k)}$ in the N-SFEM. In addition, it also makes the implementation procedure and the programming much easier. As a result, the coding can be largely same as the standard FEM.

Applying the node-based smoothing operation, the *compatible* strains $\boldsymbol{\varepsilon} = \nabla_s \mathbf{u}$ used in Eq. (1) is used to create a *smoothed* strain on the cell $\Omega^{(k)}$ associated with node k:

$$\tilde{\boldsymbol{\varepsilon}}_k = \int_{\Omega^{(k)}} \boldsymbol{\varepsilon}(\mathbf{x})\Phi_k(\mathbf{x})\,\mathrm{d}\Omega = \int_{\Omega^{(k)}} \nabla_s \mathbf{u}(\mathbf{x})\Phi_k(\mathbf{x})\,\mathrm{d}\Omega, \tag{8}$$

where $\Phi_k(\mathbf{x})$ is a given smoothing function that satisfies at least unity property

$$\int_{\Omega^{(k)}} \Phi_k(\mathbf{x})\,\mathrm{d}\Omega = 1. \tag{9}$$

Using the following constant smoothing function

$$\Phi_k(\mathbf{x}) = \begin{cases} 1/V^{(k)} & \mathbf{x} \in \Omega^{(k)}, \\ 0 & \mathbf{x} \notin \Omega^{(k)}, \end{cases} \tag{10}$$

where $V^{(k)}$ is the area/volume of the cell $\Omega^{(k)}$ and is calculated by

$$V^{(k)} = \int_{\Omega^{(k)}} \mathrm{d}\Omega = \frac{1}{3}\sum_{i=1}^{N_e^{(k)}} V_e^{(i)} \quad \text{for triangular element}, \tag{11}$$

$$V^{(k)} = \int_{\Omega^{(k)}} \mathrm{d}\Omega = \frac{1}{4}\sum_{i=1}^{N_e^{(k)}} V_e^{(i)} \quad \text{for tetrahedral element}, \tag{12}$$

where $N_e^{(k)}$ is the number of elements around the node k and $V_e^{(i)}$ is the area/volume of the ith element around the node k.

In the N-SFEM-T3 and N-SFEM-T4, the trial function $\mathbf{u}^h(\mathbf{x})$ is the same as in Eq. (2) of the FEM and therefore the force vector $\mathbf{f}$ in the N-SFEM-T3 and N-SFEM-T4 is calculated in the same way as in the FEM.

Substituting Eq. (2) into Eq. (8), the smoothed strain on the cell $\Omega^{(k)}$ associated with node k can be written in the following matrix form of nodal displacements

$$\tilde{\boldsymbol{\varepsilon}}_k = \sum_{I \in N_n^{(k)}} \widetilde{\mathbf{B}}_I(\mathbf{x}_k)\mathbf{d}_I, \tag{13}$$

where $N_n^{(k)}$ is the number of nodes that are directly connected to node k and $\widetilde{\mathbf{B}}_I(\mathbf{x}_k)$, that is termed as the *smoothed strain matrix* on the cell $\Omega^{(k)}$, is calculated numerically by an assembly process similarly as in the FEM

$$\widetilde{\mathbf{B}}_I(\mathbf{x}_k) = \frac{1}{V^{(k)}}\sum_{i=1}^{N_e^{(k)}} \frac{1}{3} V_e^{(i)} \mathbf{B}_i \quad \text{for the triangular elements}, \tag{14}$$

$$\widetilde{\mathbf{B}}_I(\mathbf{x}_k) = \frac{1}{V^{(k)}}\sum_{i=1}^{N_e^{(k)}} \frac{1}{4} V_e^{(i)} \mathbf{B}_i \quad \text{for the tetrahedral elements}, \tag{15}$$

where $\mathbf{B}_i$ is the strain gradient matrix of the ith element around the node k.

Due to the use of the triangular or tetrahedral elements with the linear shape functions, the entries of matrix $\mathbf{B}_i$ are constants, and so are the entries of matrix $\widetilde{\mathbf{B}}_I(\mathbf{x}_k)$. The entries in sub-matrices of the stiffness matrix $\widetilde{\mathbf{K}}$ of the system is then assembled by a similar process as in the FEM

$$\widetilde{\mathbf{K}}_{IJ} = \sum_{k=1}^{N_n} \widetilde{\mathbf{K}}_{IJ(k)}, \tag{16}$$

where $\widetilde{\mathbf{K}}_{IJ(k)}$ is the stiffness matrix associated with node k and is calculated by

$$\widetilde{\mathbf{K}}_{IJ(k)} = \int_{\Omega^{(k)}} \widetilde{\mathbf{B}}_I^{\mathrm{T}} \mathbf{D} \widetilde{\mathbf{B}}_J \, \mathrm{d}\Omega = \widetilde{\mathbf{B}}_I^{\mathrm{T}} \mathbf{D} \widetilde{\mathbf{B}}_J V^{(k)}. \tag{17}$$

Note that with this formulation, only the area/volume and the usual compatible strain matrices $\mathbf{B}_i$ of triangular or tetrahedral elements are needed to calculate the system stiffness matrix for the N-SFEM. The procedure of dividing each triangular and tetrahedral element into three or four sub-domains of equal area in the N-SFEM-T3 and N-SFEM-T4 presented above is only to demonstrate the process of formulation. Therefore, no explicit formation of four equal sub-domains of the tetrahedral element in the N-SFEM-T4 is necessary in the actual implementation and coding.

2.3. An alpha finite element method for triangular elements (αFEM-T3) for 2D problems

The αFEM-T3 combines both the N-SFEM-T3 and the standard FEM-T3 by using the scale factor $\alpha \in [0,1]$. As presented in the previous subsection, in the N-SFEM-T3, the area of each triangle is divided into three quadrilaterals of equal area and each quadrilateral is used to calculate the contribution to the stiffness matrix of the node attached to the quadrilateral as shown in Fig. 2. In the αFEM-T3, the area V_e of triangular element is divided into four parts with a scale factor α as shown in Fig. 2: three quadrilaterals scaled down by $(1-\alpha^2)$ at three corners with equal area of $\frac{1-\alpha^2}{3} V_e$, and the remaining Y-shaped part in the middle of the element of area $\alpha^2 V_e$. The N-SFEM-T3 is used to calculate for three quadrilaterals at the three corners, while the FEM-T3 is used to calculate for the Y-shaped area. The entries in sub-matrices of the system stiffness matrix $\mathbf{K}^{\alpha\text{FEM-T3}}$ will be the assembly from the entries of those of both the N-SFEM-T3 and the FEM-T3 as follows:

$$\mathbf{K}_{IJ}^{\alpha\text{FEM-T3}} = \sum_{k=1}^{N_n} \mathbf{K}_{IJ(k)}^{\text{N-SFEM-T3}} + \sum_{l=1}^{N_e} \mathbf{K}_{IJ(l)}^{\text{FEM}}, \tag{18}$$

where N_e is the number of total elements in the entire problem domain and

$$\mathbf{K}_{IJ(k)}^{\text{N-SFEM-T3}} = \int_{\Omega^{(k,\alpha)}} (\widetilde{\mathbf{B}}_I^{(\alpha)}(\mathbf{x}_k))^{\mathrm{T}} \mathbf{D} \widetilde{\mathbf{B}}_J^{(\alpha)}(\mathbf{x}_k) \, \mathrm{d}\Omega \tag{19}$$

$$\mathbf{K}_{IJ(l)}^{\text{FEM}} = \int_{\Omega_e^{(\alpha)}} \mathbf{B}_I^{\mathrm{T}} \mathbf{D} \mathbf{B}_J \, \mathrm{d}\Omega = \mathbf{B}_I^{\mathrm{T}} \mathbf{D} \mathbf{B}_J \alpha^2 V_e \tag{20}$$

in which $\Omega_e^{(\alpha)}$ is the Y-shape area of triangle; $\Omega^{(k,\alpha)}$ is the area associated the node k and bounded by the boundary $\Gamma^{(k,\alpha)}$ as shown in Fig. 3. The smoothed strain matrix $\widetilde{\mathbf{B}}_I^{(\alpha)}(\mathbf{x}_k)$ for $\Omega^{(k,\alpha)}$ is calculated by

$$\widetilde{\mathbf{B}}_I^{(\alpha)}(\mathbf{x}_k) = \frac{1}{V^{(k,\alpha)}} \sum_{i=1}^{N_e^{(k)}} \frac{1}{3}(1-\alpha^2) V_e^{(i)} \mathbf{B}_i = \frac{1}{V^{(k)}} \sum_{i=1}^{N_e^{(k)}} \frac{1}{3} V_e^{(i)} \mathbf{B}_i = \widetilde{\mathbf{B}}_I(\mathbf{x}_k), \tag{21}$$

which implies that we can use the matrix $\widetilde{\mathbf{B}}_I(\mathbf{x}_k)$ for area $\Omega^{(k)}$ bounded by the boundary $\Gamma^{(k)}$ instead the matrix $\widetilde{\mathbf{B}}_I^{(\alpha)}(\mathbf{x}_k)$ for area $\Omega^{(k,\alpha)}$ in the calculation. Note that to obtain Eq. (21), the following relation between the area $V^{(k,\alpha)}$ of the area $\Omega^{(k,\alpha)}$ and the area $V^{(k)}$ of the area $\Omega^{(k)}$ is used:

$$V^{(k,\alpha)} = \int_{\Omega^{(k,\alpha)}} \mathrm{d}\Omega = \sum_{i=1}^{N_e^{(k)}} \frac{1}{3}(1-\alpha^2) V_e^{(i)} = (1-\alpha^2) V^{(k)}. \tag{22}$$

Using Eqs. (21) and (22), Eq. (19) now is written as

$$\mathbf{K}_{IJ(k)}^{\text{N-SFEM-T3}} = (1-\alpha^2) \widetilde{\mathbf{B}}_I^{\mathrm{T}} \mathbf{D} \widetilde{\mathbf{B}}_J V^{(k)}, \tag{23}$$

which implies that we can simplify the procedure of coding program of the αFEM-T3 by using the original N-SFEM-T3 in which each triangle only needs to be divided into three quadrilaterals of equal area to calculate entries of the stiffness matrix and then multiply $(1-\alpha^2)$.

To calculate Eq. (20), the standard FEM using triangular elements is used to calculate the entries of the stiffness matrix and then the parameter α^2 is multiplied.

Now, the αFEM-T3 is equipped with a scaling factor α that acts as a knob controlling the contributions from the N-SFEM-T3 and the FEM. When the factor α varies from 0 to 1, a continuous solution function from the solution of the N-SFEM to that of the FEM is obtained.

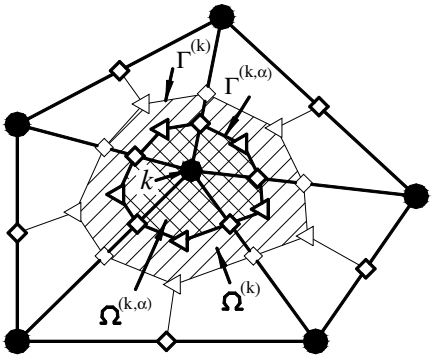

Fig. 3. Cell associated with nodes for triangular elements in the αFEM-T3.

2.4. An alpha finite element method for tetrahedral elements (αFEM-T4) for 3D problems

Following the same concept of the αFEM-T3, we develop a tetrahedral element for αFEM for 3D problems (αFEM-T4). The volume V_e of each tetrahedral element will be divided into five parts based on the scale factor α: four volumes at four corners with equal volume of $\frac{(1-\alpha^3)}{4} V_e$ and the remaining part in the middle of the element of volume $\alpha^3 V_e$. The N-SFEM is used to calculate for four corner parts of equal volumes, while the FEM-T4 is used to calculate for

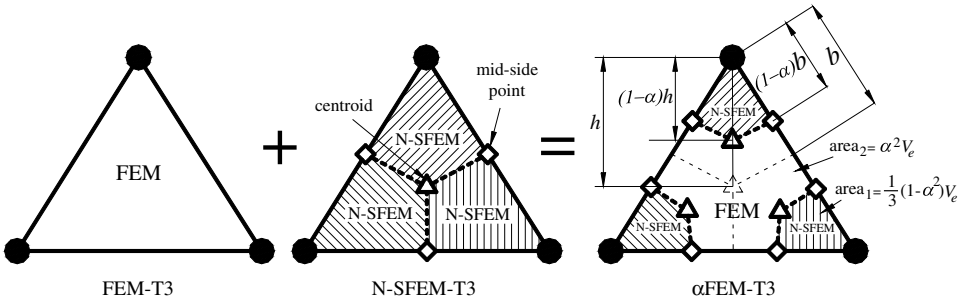

Fig. 2. An αFEM-T3 element: combination of the triangular elements of FEM and N-SFEM. N-SFEM is used for three quadrilaterals, and FEM is used for the Y-shaped area in the center.

the remaining volume in the middle. The system stiffness matrix $\mathbf{K}^{\alpha\text{FEM-T4}}$ is then calculated using

$$\mathbf{K}_{IJ}^{\alpha\text{FEM-T4}} = \sum_{k=1}^{N_n} \mathbf{K}_{IJ(k)}^{\text{N-SFEM-T4}} + \sum_{l=1}^{N_e} \mathbf{K}_{IJ(l)}^{\text{FEM-T4}} \tag{24}$$

with the matrices $\mathbf{K}_{IJ(k)}^{\text{N-SFEM-T4}}$ and $\mathbf{K}_{IJ(l)}^{\text{FEM-T4}}$ calculated as follows:

$$\mathbf{K}_{IJ(k)}^{\text{N-SFEM-T4}} = (1-\alpha^3)\widetilde{\mathbf{B}}_I^{\mathrm{T}}\mathbf{D}\widetilde{\mathbf{B}}_J V^{(k)} \tag{25}$$

$$\mathbf{K}_{IJ(l)}^{\text{FEM-T4}} = \int_{\Omega_e^{(\alpha)}} \mathbf{B}_I^{\mathrm{T}}\mathbf{D}\mathbf{B}_J \,\mathrm{d}\Omega = \mathbf{B}_I^{\mathrm{T}}\mathbf{D}\mathbf{B}_J \alpha^3 V_e \tag{26}$$

in which $\Omega_e^{(\alpha)}$ is the remaining volume in the middle of the element; the smoothed strain matrix $\widetilde{\mathbf{B}}_I$ is calculated using Eq. (15), $V^{(k)}$ is calculated using Eq. (12) and the compatible strain matrix $\mathbf{B}_I$ is calculated using Eq. (6).

3. Properties of the αFEM-T3 and αFEM-T4

In the case of homogeneous essential boundary conditions, the αFEM-T3 and αFEM-T4 will have the following important properties

Property 1 (displacement compatibility). *The assumed displacement field is compatible (linearly continuous through out the domain) in the αFEM-T3 and αFEM-T4. This property can be explicitly seen from the αFEM-T3 and αFEM-T4 formulation procedure: linear element based interpolation is used through out the entire problem domain. This property ensures that the αFEM-T3 and αFEM-T4 for any $\alpha \in [0,1]$ will be able to reproduce exactly the linear field. This will be confirmed in the patch tests given in Section 5.*

Property 2 (variational consistence). *The αFEM-T3 (or αFEM-T4) is variationally consistent.*

Proof. In the αFEM-T3, besides the compatible strain $\varepsilon = \nabla_s \mathbf{u}$ is used for N_eY-shaped areas $\Omega_e^{(\alpha)}$ of elements, the smoothed strain (8) is used for N_n smoothing cells $\Omega^{(k,\alpha)}$ associated with N_n nodes in the *generalized* Galerkin weak form, the variational consistency thus needs to be examined. To this end, we start with the modified Hellinger–Reissner variational principle [28] with the assumed strain vector $\tilde{\boldsymbol{\varepsilon}}$ and displacements $\mathbf{u}$ as independent field variables in which note that $\tilde{\boldsymbol{\varepsilon}} = \boldsymbol{\varepsilon}$ for N_eY-shaped areas $\Omega_e^{(\alpha)}$ of elements:

$$U(\mathbf{u},\tilde{\boldsymbol{\varepsilon}}) = -\int_\Omega \frac{1}{2}\tilde{\boldsymbol{\varepsilon}}^{\mathrm{T}}\mathbf{D}\tilde{\boldsymbol{\varepsilon}}\,\mathrm{d}\Omega + \int_\Omega (\mathbf{D}\tilde{\boldsymbol{\varepsilon}})^{\mathrm{T}}(\nabla_s\mathbf{u})\,\mathrm{d}\Omega - \int_\Omega \mathbf{u}^{\mathrm{T}}\mathbf{b}\,\mathrm{d}\Omega - \int_{\Gamma_t}\mathbf{u}^{\mathrm{T}}\bar{\mathbf{t}}\,\mathrm{d}\Gamma. \tag{27}$$

Performing the variation using the chain rule, one obtains

$$\begin{aligned}\delta U(\mathbf{u},\tilde{\boldsymbol{\varepsilon}}) = &-\int_\Omega \delta\tilde{\boldsymbol{\varepsilon}}^{\mathrm{T}}\mathbf{D}\tilde{\boldsymbol{\varepsilon}}\,\mathrm{d}\Omega + \int_\Omega \delta\tilde{\boldsymbol{\varepsilon}}^{\mathrm{T}}\mathbf{D}(\nabla_s\mathbf{u})\,\mathrm{d}\Omega + \int_\Omega \tilde{\boldsymbol{\varepsilon}}^{\mathrm{T}}\mathbf{D}(\nabla_s\delta\mathbf{u})\,\mathrm{d}\Omega \\ &- \int_\Omega \delta\mathbf{u}^{\mathrm{T}}\mathbf{b}\,\mathrm{d}\Omega - \int_{\Gamma_t}\delta\mathbf{u}^{\mathrm{T}}\bar{\mathbf{t}}\,\mathrm{d}\Gamma = 0.\end{aligned} \tag{28}$$

Discretizing the domain Ω into N_e triangles Ω_e including N_n smoothing cells $\Omega^{(k,\alpha)}$ associated with N_n nodes and N_e Y-shaped areas $\Omega_e^{(\alpha)}$ corresponding to the N_e elements, and then substituting the approximations (2) and (13) into (28) and using the arbitrary property of variation, we obtain

$$\mathbf{K}^{\text{two-field}}\mathbf{d} = \mathbf{f}, \tag{29}$$

where $\mathbf{K}^{\text{two-field}}$ is the *smoothed* stiffness matrix and $\mathbf{f}$ is the element force vector given by

$$\begin{aligned}\mathbf{K}_{IJ}^{\text{two-field}} = &-\int_{\Omega^{(k,\alpha)}} (\widetilde{\mathbf{B}}_I^{\alpha})^{\mathrm{T}}\mathbf{D}\widetilde{\mathbf{B}}_J^{\alpha}\,\mathrm{d}\Omega + 2\int_{\Omega^{(k,\alpha)}} (\widetilde{\mathbf{B}}_I^{\alpha})^{\mathrm{T}}\mathbf{D}\mathbf{B}_J\,\mathrm{d}\Omega \\ &- \int_{\Omega_e^{(\alpha)}} (\widetilde{\mathbf{B}}_I^{\alpha})^{\mathrm{T}}\mathbf{D}\widetilde{\mathbf{B}}_J^{\alpha}\,\mathrm{d}\Omega + 2\int_{\Omega_e^{(\alpha)}} (\widetilde{\mathbf{B}}_I^{\alpha})^{\mathrm{T}}\mathbf{D}\mathbf{B}_J\,\mathrm{d}\Omega,\end{aligned} \tag{30}$$

$$\mathbf{f}_I = \int_{\Omega_e} \mathbf{N}_I^{\mathrm{T}}(\mathbf{x})\mathbf{b}\,\mathrm{d}\Omega + \int_{\Gamma_t}\mathbf{N}_I^{\mathrm{T}}(\mathbf{x})\bar{\mathbf{t}}\,\mathrm{d}\Gamma. \tag{31}$$

Due to $\tilde{\boldsymbol{\varepsilon}} = \boldsymbol{\varepsilon}$ for N_eY-shaped areas $\Omega_e^{(\alpha)}$ of elements, the smoothed strain matrix $\widetilde{\mathbf{B}}_I^{\alpha}$ is also the standard compatible strain matrix $\mathbf{B}_I$, then Eq. (30) becomes

$$\begin{aligned}\mathbf{K}_{IJ}^{\text{two-field}} = &-\int_{\Omega^{(k,\alpha)}} (\widetilde{\mathbf{B}}_I^{\alpha})^{\mathrm{T}}\mathbf{D}\widetilde{\mathbf{B}}_J^{\alpha}\,\mathrm{d}\Omega + 2\int_{\Omega^{(k,\alpha)}} (\widetilde{\mathbf{B}}_I^{\alpha})^{\mathrm{T}}\mathbf{D}\mathbf{B}_J(\mathbf{x})\,\mathrm{d}\Omega \\ &+ \int_{\Omega_e^{(\alpha)}} \mathbf{B}_I^{\mathrm{T}}\mathbf{D}\mathbf{B}_J\,\mathrm{d}\Omega.\end{aligned} \tag{32}$$

Using smoothed matrices $\widetilde{\mathbf{B}}_I$ in Eq. (14) for N_n smoothing cells $\Omega^{(k,\alpha)}$ associated with N_n nodes, we have

$$\begin{aligned}\int_{\Omega^{(k,\alpha)}} \widetilde{\mathbf{B}}_I^{\mathrm{T}}\mathbf{D}\mathbf{B}_J(\mathbf{x})\,\mathrm{d}\Omega &= \widetilde{\mathbf{B}}_I^{\mathrm{T}}\mathbf{D}\int_{\Omega^{(k,\alpha)}} \mathbf{B}_J(\mathbf{x})\,\mathrm{d}\Omega \\ &= \widetilde{\mathbf{B}}_I^{\mathrm{T}}\mathbf{D}A^{(k,\alpha)}\int_{\Omega^{(k,\alpha)}} \frac{\mathbf{B}_J(\mathbf{x})}{A^{(k,\alpha)}}\,\mathrm{d}\Omega = \widetilde{\mathbf{B}}_I^{\mathrm{T}}\mathbf{D}\widetilde{\mathbf{B}}_J A^{(k,\alpha)} \\ &= \int_{\Omega^{(k,\alpha)}} \widetilde{\mathbf{B}}_I^{\mathrm{T}}\mathbf{D}\widetilde{\mathbf{B}}_J\,\mathrm{d}\Omega,\end{aligned} \tag{33}$$

which means that the following orthogonal condition is satisfied [29]

$$\int_{\Omega^{(k,\alpha)}} \widetilde{\mathbf{B}}_I^{\mathrm{T}}\mathbf{D}\mathbf{B}_J(\mathbf{x})\,\mathrm{d}\Omega = \int_{\Omega^{(k,\alpha)}} \widetilde{\mathbf{B}}_I^{\mathrm{T}}\mathbf{D}\widetilde{\mathbf{B}}_J\,\mathrm{d}\Omega \tag{34}$$

then Eq. (32) becomes

$$\mathbf{K}_{IJ}^{\text{two-field}} = \int_{\Omega^{(k,\alpha)}} (\widetilde{\mathbf{B}}_I^{\alpha})^{\mathrm{T}}\mathbf{D}\widetilde{\mathbf{B}}_J^{\alpha}\,\mathrm{d}\Omega + \int_{\Omega_e^{(\alpha)}} \mathbf{B}_I^{\mathrm{T}}\mathbf{D}\mathbf{B}_J\,\mathrm{d}\Omega. \tag{35}$$

The αFEM-T3 uses directly Eq. (35) to calculate the stiffness matrix, therefore, the αFEM-T3 is "variationally consistent". This proof is applicable also the same for the αFEM-T4.

Note that although the two-field Hellinger-Reissner principle is used, the αFEM has only the displacements as unknowns. Therefore, it is very much different from the so-called mixed FEM formulation, where stresses (or strains) are usually also unknowns. □

Property 3 (lower bound property). *When $\alpha = 1.0$, the αFEM-T3 and αFEM-T4 become the standard FEM. The strain energy $E(\alpha = 1)$ is an underestimation of the exact strain energy.*

Property 4 (upper bound property). *When $\alpha = 0.0$, the αFEM-T3 and αFEM-T4 becomes the N-SFEM. The strain energy $E(\alpha = 0)$ is an overestimation of the exact strain energy.*

A proof procedure and arguments that shows the same upper bound property of the LC-PIM can be found in Ref. [15]. An intuitive explanation on why the N-SFEM can always produce upper bound solution was also presented in Ref. [14]. The numerical examples in Section 6 of this paper will confirm the property without any exception.

Property 5 (solution continuity property). *When α changes from 0.0 to 1.0, the solutions of the αFEM-T3 and αFEM-T4 are continuous functions of α from the solution of the N-SFEM and that of the standard FEM.*

Property 6 (exact solution property). *The exact solution in strain energy exactly falls in the range of the αFEM-T3 and αFEM-T4 with $\alpha \in [0,1]$. This means that the exact solution in strain energy can be obtained using the αFEM-T3 and αFEM-T4 with an $\alpha_{\text{exact}} \in [0,1]$.*

This property is a natural outcome of the Property 3–5. Based on 6, one can devise the following procedure to compute the exact solution in strain energy.

Our numerical study has shown that using the meshes with the same aspect ratio, the strain energy curves $E(\alpha)$ corresponding to these meshes will intersect at a common point (α_{exact}, E_{exact}) which gives the nearly exact strain energy of the problem. The corresponding displacement solution of the αFEM-T3 and αFEM-T4 at α_{exact} for the meshes with the same aspect ratio is also much better than those of either the standard FEM or the N-SFEM. This procedure will be used in numerical examples to obtain nearly exact solutions in strain energy.

Note that the meshes with the same aspect ratio are defined in two ways: one for regular meshes and one for irregular meshes. For regular meshes which are usually used only for the regular domains, the ratio of number of elements discretized along coordinate directions has to be the same. For example, for the rectangular 2D meshes, the same aspect ratio of three meshes (16 × 4), (32 × 8) and (64 × 16) is 4. For irregular meshes used for any domains, the meshes with the same aspect ratio are obtained by dividing each element of the initial coarse mesh into 2^2, 3^2, 4^2, etc. equal elements for triangular elements, and into 2^3, 3^3, 4^3, etc. equal elements for tetrahedral elements. The refinement from the initial coarse mesh to obtain the meshes with the same aspect ratio is available in many automatic programs creating three-node triangular and four-node tetrahedral elements without any difficulty. Note that, we do not require the elements in a mesh to have the same aspect ratio. We require only two consequent meshes to have the same aspect ratio.

Property 7. *The stiffness matrix of the αFEM-T3 (or αFEM-T4) has the same unknowns of only the displacement, the same bandwidth and sparsity as that of the standard FEM, and hence the same computational complexity.*

Property 8. *For the nearly incompressible case (ν approaches to 0.5) in the plane strain problem, the volumetric locking can be solved by using $\alpha = 0$ or a very small $\alpha = 0.5 - \nu$ for the proposed elements, where ν is the Poisson's ratio that is smaller but very close to 0.5. Note that, for this kind of problems, we have to give up on the "exact" solution, and only focus on solving the volumetric locking.*

In the above formulation of the αFEM-T3 (or αFEM-T4), only the area (or volume), the usual compatible strain matrices $\mathbf{B}_I$ of triangular (or tetrahedral) elements together the factor α are needed to calculate the system stiffness matrix. In the actual programming, the standard FEM and the N-SFEM-T3 (or N-SFEM-T4) formulae are used directly to calculate the entries of the stiffness matrices and then the results obtained are scaled by α^2 and $(1-\alpha^2)$, respectively, as shown in Eqs. (20) and (23) for the αFEM-T3 (or by α^3 and $(1-\alpha^3)$, respectively, as shown in Eqs. (25) and (26) for the αFEM-T4). Therefore, our αFEM-T3 (or αFEM-T4) code is very similar to a standard FEM code, and the bandwidth or sparsity of the stiffness matrix of αFEM-T3 (or αFEM-T4) and that of FEM is exactly the same. The CPU cost for solving the system equations will also be largely the same.

4. Numerical implementation

4.1. Exact solution for linear mechanics problems

Numerical procedure for computing the exact solution using the αFEM-T3 and αFEM-T4 can be summarized as follows:

1. Discretize the domain Ω into two sets of mesh of coarse triangular (for 2D problems) or tetrahedral (for 3D problems) elements with the same aspect ratio.
2. Choose one array of $\alpha \in \overline{0:1}$, for example $\alpha = [0.0\ 0.2\ \cdots\ 0.8\ 1.0]^{\mathrm{T}}$.
3. Loop over two sets of mesh created in step 1.
4. Loop over the array of $\alpha \in \overline{0:1}$.
5. Loop over all the elements (use the standard FEM):
   - Compute and save the gradient matrix **B** of the element by Eq. (6).
   - Evaluate the stiffness matrix and force vector of the element by Eqs. (7) and (5).
   - Multiply the stiffness matrix of the element with α^2 for triangular elements by Eq. (20) or with α^3 for tetrahedral elements by Eq. (26) and then assemble into the global stiffness matrix.
   - Assemble force vector into the global force vector.
6. End the loop over all the elements.
7. Loop over all the nodes (use the N-SFEM-T3):
   - Use the gradient matrices **B** of the element saved in step 5 to compute the gradient matrix $\widetilde{\mathbf{B}}$ of the node by Eq. (14) for the triangular elements or by Eq. (15) for the tetrahedral elements.
   - Evaluate the stiffness matrix of the node by Eq. (17).
   - Multiply the stiffness matrix of the node with $(1-\alpha^2)$ for triangular elements by Eq. (23) or $(1-\alpha^3)$ for tetrahedral elements by Eq. (25) and then assemble into the global stiffness matrix.
8. End the loop over all the nodes.
9. Implement essential boundary conditions.
10. Solve the system equations for the nodal displacements.
11. Evaluate strain, stress and save the global strain energy.
12. End the loop over the array containing $\alpha \in \overline{0:1}$.
13. End the loop over two sets of coarse meshes.
14. Interpolate the exact strain energy at α_{exact} from two arrays containing the strain energies saved at step 11.
15. Use α_{exact} and a finer discretization with the same aspect ratio as the two coarse meshes to calculate the desired solution through steps from 5 to 11.

Note that, if we only need to improve the accuracy of solution, it is recommended to use directly an $\alpha \in \overline{0.5:0.7}$ for any meshes without knowing α_{exact}. This range of $\alpha \in \overline{0.5:0.7}$ is found by numerical "experiments" on different linear problems using the αFEM-T3 and αFEM-T4. By this way, the α chosen may not be optimal and the solution may not be exact, but the accuracy of the solution is often much better than FEM.

Based on the theory presented, we know that in any case, the accuracy (in energy norm) of the proposed method is always better than either FEM or N-SFEM for any $\alpha \in (0,1)$. This gives us a guarantee that we can only get a better solution using any $\alpha \in (0,1)$.

4.2. Volumetric locking problems

As presented at Property 8 in Section 3, it is recommended to use $\alpha = 0$ or a very small $\alpha = 0.5 - \nu$ for the proposed elements, where ν is the Poisson's ratio that is smaller but very close to 0.5. One numerical example about this will be performed in Section 6.

4.3. Nonlinear problems of large deformation

For the nonlinear problems of large deformation, the values of the strain gradient matrices and stresses at the nodes are the average values of those of the adjacent elements around the node, and all the techniques used in the FEM can be employed. The finite element model of the αFEM-T3 for nonlinear problems of large deformation based on the total Lagrange formulation [22,27] is expressed as follows:

$$(\mathbf{K}_L^{\alpha\text{FEM}} + \mathbf{K}_{\text{NL}}^{\alpha\text{FEM}})\mathbf{d} = \mathbf{f} - \mathbf{f}_1, \tag{36}$$

where

$$\mathbf{K}_L^{\alpha\text{FEM}} = \sum_{k=1}^{N_n}(1-\alpha^2)\widetilde{\mathbf{B}}_L^{\mathrm{T}}\mathbf{D}\widetilde{\mathbf{B}}_L V^{(k)} + \sum_{e=1}^{N_e}\alpha^2\mathbf{B}_L^{\mathrm{T}}\mathbf{D}\mathbf{B}_L V_e \tag{37}$$

$$\mathbf{K}_{\text{NL}}^{\alpha\text{FEM}} = \sum_{k=1}^{N_n}(1-\alpha^2)\widetilde{\mathbf{B}}_{\text{NL}}^{\mathrm{T}}\widetilde{\mathbf{S}}\widetilde{\mathbf{B}}_{\text{NL}} V^{(k)} + \sum_{e=1}^{N_e}\alpha^2\mathbf{B}_{\text{NL}}^{\mathrm{T}}\mathbf{S}\mathbf{B}_{\text{NL}} V_e \tag{38}$$

$$\mathbf{f}_1 = \sum_{k=1}^{N_n}(1-\alpha^2)\widetilde{\mathbf{B}}_L^{\mathrm{T}}\{\widetilde{\mathbf{S}}\} V^{(k)} + \sum_{e=1}^{N_e}\alpha^2\mathbf{B}_L^{\mathrm{T}}\{\mathbf{S}\} V_e \tag{39}$$

with

$$\mathbf{B}_L = \begin{bmatrix} F_{11}N_{1,1} & F_{21}N_{1,1} & F_{11}N_{2,1} & F_{21}N_{2,1} & F_{11}N_{3,1} & F_{21}N_{3,1} \\ F_{12}N_{1,2} & F_{22}N_{1,2} & F_{12}N_{2,2} & F_{22}N_{2,2} & F_{12}N_{3,2} & F_{22}N_{3,2} \\ F_{11}N_{1,2}+F_{12}N_{1,1} & F_{21}N_{1,2}+F_{22}N_{1,1} & F_{11}N_{2,2}+F_{12}N_{2,1} & F_{21}N_{2,2}+F_{22}N_{2,1} & F_{11}N_{3,2}+F_{12}N_{3,1} & F_{21}N_{3,2}+F_{22}N_{3,1} \end{bmatrix}, \tag{40}$$

$$\widetilde{\mathbf{B}}_L = \frac{1}{V^{(k)}} \sum_{i=1}^{N_e^{(k)}} \frac{1}{3} V_e^{(i)} \mathbf{B}_L^{(i)}, \tag{41}$$

$$\mathbf{B}_{\mathrm{NL}} = \begin{bmatrix} N_{1,1} & 0 & N_{2,1} & 0 & N_{3,1} & 0 \\ N_{1,2} & 0 & N_{2,2} & 0 & N_{3,2} & 0 \\ 0 & N_{1,1} & 0 & N_{2,1} & 0 & N_{3,1} \\ 0 & N_{1,2} & 0 & N_{2,2} & 0 & N_{3,2} \end{bmatrix} \quad \text{and} \tag{42}$$

$$\widetilde{\mathbf{B}}_{\mathrm{NL}} = \frac{1}{V^{(k)}} \sum_{i=1}^{N_e^{(k)}} \frac{1}{3} V_e^{(i)} \mathbf{B}_{\mathrm{NL}}^{(i)},$$

$$\mathbf{S} = \begin{bmatrix} S_{11} & S_{12} & 0 & 0 \\ S_{12} & S_{22} & 0 & 0 \\ 0 & 0 & S_{11} & S_{12} \\ 0 & 0 & S_{12} & S_{22} \end{bmatrix} \quad \text{and} \quad \widetilde{\mathbf{S}} = \frac{1}{V^{(k)}} \sum_{i=1}^{N_e^{(k)}} \frac{1}{3} V_e^{(i)} \mathbf{S}^{(i)}, \tag{43}$$

where the second Piola–Kirchhoff stress tensor $\{\mathbf{S}\}$ is derived from

$$\{\mathbf{S}\} = \begin{bmatrix} S_{11} \\ S_{22} \\ S_{12} \end{bmatrix} = \mathbf{D} \begin{bmatrix} E_{11} \\ E_{22} \\ 2E_{12} \end{bmatrix} \quad \text{and} \quad \{\widetilde{\mathbf{S}}\} = \frac{1}{V^{(k)}} \sum_{i=1}^{N_e^{(k)}} \frac{1}{3} V_e^{(i)} \{\mathbf{S}\}^{(i)} \tag{44}$$

with the Green–Lagrange strain tensor $\mathbf{E}$ of the elements is calculated by

$$\mathbf{E} = \begin{bmatrix} E_{11} & E_{12} \\ E_{21} & E_{22} \end{bmatrix} = \frac{1}{2}(\mathbf{F}^{\mathrm{T}}\mathbf{F} - \mathbf{I}), \tag{45}$$

where $\mathbf{I}$ is the second order unit matrix and the deformation gradient tensor $\mathbf{F}$ of the elements is derived from

$$\mathbf{F} = \begin{bmatrix} F_{11} & F_{12} \\ F_{21} & F_{22} \end{bmatrix} = \left(\frac{\partial \mathbf{x}}{\partial \mathbf{X}}\right)^{\mathrm{T}} = (\nabla \mathbf{d} + \mathbf{I})^{\mathrm{T}}. \tag{46}$$

Note that in Eq. (40) and (42), $N_{I,j} = \frac{\partial N_I}{\partial X_j}$.

For nonlinear problems of large deformation, it is generally difficult to obtain the "exact" solution. Our aim is thus to improve the accuracy of the solution. Similarly to linear problems, it is recommended that an $\alpha \in \overline{0.5 : 0.7}$ is used directly for nonlinear problems of large deformation. For such an α, the accuracy of the solution is often much better than FEM. In other way, we can also use the optimal value α obtained from the small deformation problem based on the scaled meshes and apply for large deformation. By this way, the α chosen is not optimal for the nonlinear problem and we will not obtain the exact solution, but it still much better than the pure FEM solution.

The formulation presented above is straightforward to extend to the αFEM-T4 for 3D problems using tetrahedral elements. Two numerical examples about this will be performed in Section 6.

5. Standard patch tests

5.1. Standard patch test for 2D problems

Satisfaction of the standard patch test requires that the displacements of all the interior nodes follow "exactly" (to machine precision) the same linear function of the imposed displacements on the edges of the patch. An irregular domain discretization of a square patch using 58 three-node triangular elements is shown in Fig. 4.

The parameters are taken as $E = 100$, $\nu = 0.3$ and linear displacement field is given by

$$\begin{aligned} u &= x, \\ v &= y. \end{aligned} \tag{47}$$

The following error norm in displacements is used to examine the computed results.

$$e_d = \frac{\sum_{i=1}^{\mathrm{ndof}} |u_i - u_i^h|}{\sum_{i=1}^{\mathrm{ndof}} |u_i|} \times 100\%, \tag{48}$$

where u_i is the exact solution and u_i^h is the numerical solution.

It is found that the αFEM-T3 can pass the standard patch test within machine precision regardless of the value of $\alpha \in [0,1]$ used as shown in Table 1. This example confirms Property 1 for 2D problems: the αFEM is *displacement* compatible and hence will always converge.

5.2. Irons first-order patch test for 3D problems

Satisfaction of the first-order patch test requires that the displacements of all the interior nodes follow "exactly" (to machine precision) the same linear function of the imposed displacement on the surfaces of the patch and constant strain/stress states are

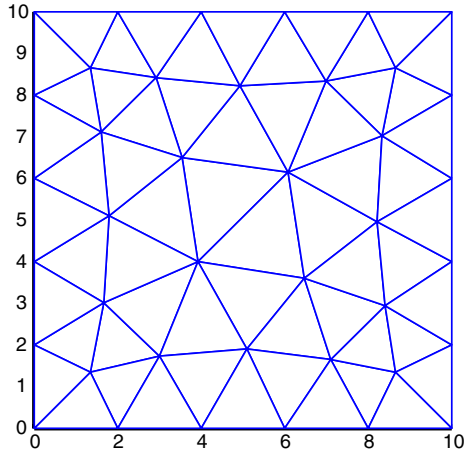

Fig. 4. Domain discretization of a square patch using three-node triangular elements.

Table 1
Displacement error norm e_d (%)

$\alpha = 0.0$ (N-SFEM)	$\alpha = 0.2$	$\alpha = 0.4105$[a]	$\alpha = 0.6038$[a]	$\alpha = 0.8$	$\alpha = 1.0$ (FEM)
0.2757 e−12	1.6029 e−12	1.4327 e−12	2.1737 e−12	0.7946 e−12	1.6499 e−12

[a] Arbitrarily generated number.

Table 2
Displacement error norm e_d (%)

	$\alpha = 0.0$ N-SFEM (tetrahedral element)	$\alpha = 0.2$	$\alpha = 0.4083$[a]	$\alpha = 0.6149$[a]	$\alpha = 0.8$	$\alpha = 1.0$ FEM
e_d (%)	0.08 e−12	0.23 e−12	0.82 e−12	1.46 e−12	13.06 e−12	0.06 e−12

[a] Arbitrarily generated number.

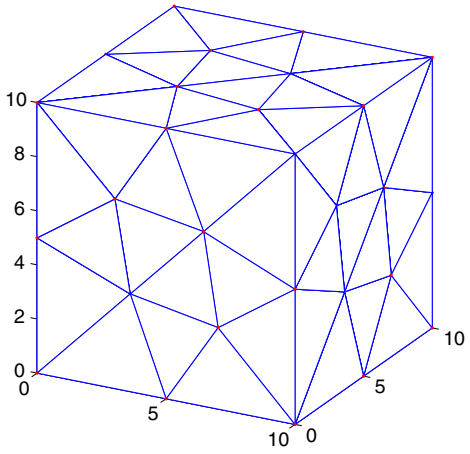

Fig. 5. Domain discretization of a cubic patch using four-node tetrahedral elements.

reproduced. An irregular spatial discretization of a cubic patch using 100 four-node tetrahedral elements is shown in Fig. 5.

The related parameters are taken as $E = 6.895 \times 10^6$ kPa, $\nu = 0.25$ and linear displacement field is given by

$$u = 0.001 * (2x + y + z)/2; \quad v = 0.001 * (x + 2y + z)/2;$$
$$w = 0.001 * (x + y + 2z)/2. \tag{49}$$

The displacement error norm is given by Eq. (48) and the energy error is defined by

$$e_e(\alpha) = |E(\alpha) - E_{\text{exact}}|, \tag{50}$$

where the total strain energy of numerical solution $E(\alpha)$ and the total strain energy of exact solution E_{exact} are calculated by

$$E(\alpha) = E^{\text{FEM}}(\alpha) + E^{\text{N-SFEM}}(\alpha) = \frac{1}{2}\sum_{i=1}^{\text{nel}} (\boldsymbol{\varepsilon}_i^h)^{\text{T}} \mathbf{D} \boldsymbol{\varepsilon}_i^h \alpha^3 V_e^{(i)} + \frac{1}{2}\sum_{k=1}^{\text{nnode}} (\tilde{\boldsymbol{\varepsilon}}_k^h)^{\text{T}} \mathbf{D} \tilde{\boldsymbol{\varepsilon}}_k^h (1-\alpha^3) V_n^{(k)}, \tag{51}$$

$$E_{\text{exact}} = \frac{1}{2}\boldsymbol{\varepsilon}^{\text{T}} \mathbf{D} \boldsymbol{\varepsilon} V_{\text{cubic}}, \tag{52}$$

where nel is the total number of element of the problem, nnode is the total number of node of the problem, $\boldsymbol{\varepsilon}$ is the strain of exact solution, $\boldsymbol{\varepsilon}_i^h$ is the strain of numerical solution of the ith element, $\tilde{\boldsymbol{\varepsilon}}_k^h$ is the smoothed strain of numerical solution at the kth node.

It is found that the αFEM-T4 can pass the standard first-order patch test within machine precision regardless of the value of $\alpha \in [0,1]$, as shown in Tables 2 and 3. There is no accuracy loss due to the choice of α value. This example confirms Property 1 for 3D problems.

6. Numerical examples

In order to study the convergence rate of the present method, two norms are used here, i.e., displacement norm and energy norm. The displacement norm is given by Eq. (48) and the energy error norm is defined by

$$e_e(\alpha) = |E(\alpha) - E_{\text{exact}}|^{1/2}, \tag{53}$$

where the total strain energy of numerical solution $E(\alpha)$ is given by Eq. (51) and the total strain energy of exact solution E_{exact} is calculated by

$$E_{\text{exact}} = \frac{1}{2}\lim_{\text{nel}\to\infty}\sum_{i=1}^{\text{nel}} \boldsymbol{\varepsilon}_i^{\text{T}} \mathbf{D} \boldsymbol{\varepsilon}_i V_e^{(i)}, \tag{54}$$

where $\boldsymbol{\varepsilon}_i$ is the strain of exact solution. In the actual computation using Eq. (54), we will use a very fine mesh (nel $\to \infty$) to calculate the "exact" strain energy E_{exact}.

6.1. Cantilever beam under a tip load: convergence study

A cantilever with length L and height D is studied as a benchmark problem here, which is subjected to a parabolic traction at the free end as shown in Fig. 6. The cantilever is assumed to have a unit thickness so that plane stress condition is valid. The analytical solution is available and can be found in a textbook by Timoshenko and Goodier [30].

$$u_x = \frac{Py}{6EI}\left[(6L - 3x)x + (2+\nu)\left(y^2 - \frac{D^2}{4}\right)\right],$$
$$u_y = -\frac{P}{6EI}\left[3\nu y^2(L-x) + (4+5\nu)\frac{D^2 x}{4} + (3L - x)x^2\right], \tag{55}$$

where the moment of inertia I for a beam with rectangular cross section and unit thickness is given by $I = \frac{D^3}{12}$.

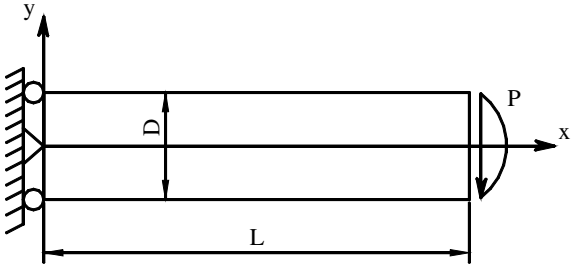

Fig. 6. Model of the cantilever loaded at the end.

Table 3
Strain energy error e_e

	$\alpha = 0.0$ N-SFEM (tetrahedral element)	$\alpha = 0.2$	$\alpha = 0.4083$[a]	$\alpha = 0.6149$[a]	$\alpha = 0.8$	$\alpha = 1.0$ FEM
e_e	2.55 e−11	2.55 e−11	2.55 e−11	2.55 e−11	2.55 e−11	2.55 e−11

[a] Arbitrarily generated number.

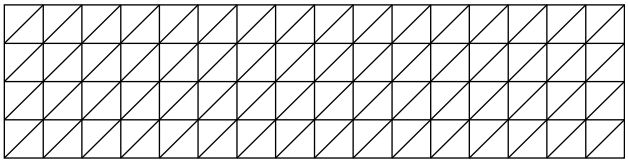

Fig. 7. Domain discretization using regular triangular elements.

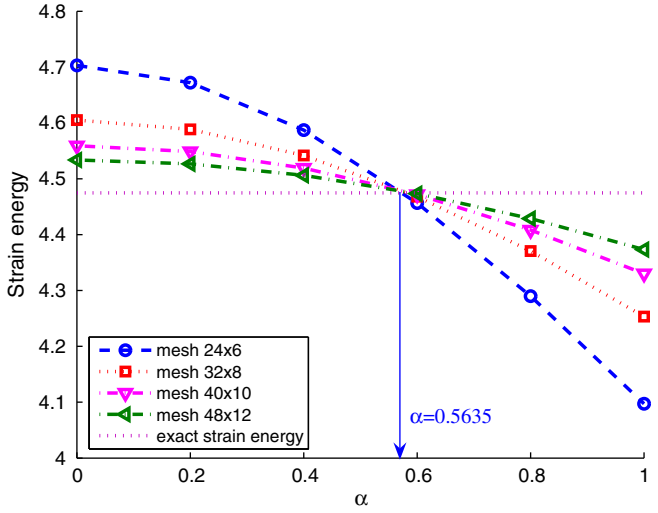

Fig. 8. Strain energy.

The stresses corresponding to the displacements Eq. (55) are

$$\sigma_{xx}(x,y) = \frac{P(L-x)y}{I}; \quad \sigma_{yy}(x,y) = 0; \quad \tau_{xy}(x,y) = -\frac{P}{2I}\left(\frac{D^2}{4} - y^2\right). \tag{56}$$

The related parameters are taken as $E = 3.0 \times 10^7$ kPa, $\nu = 0.3$, $D = 12$ m, $L = 48$ m and $P = 1000$ N. In the computations, the nodes on the left boundary are constrained using the exact displacements obtained from Eq. (55) and the loading on the right boundary uses the distributed parabolic shear stresses in Eq. (56).

In order to compare the results of the αFEM-T3 using triangular elements with those of the standard FEM using four-node quadrilateral elements that are most widely used, the regular meshes with the same aspect ratio are used. One domain discretization of these meshes is shown in Fig. 7. The exact strain energy of the problem is 4.4746. As shown in Fig. 8, the estimated strain energy at the intersection of strain energy curves are 4.4803 at $\alpha_{exact} = 0.5635$. The results are compared with the other methods: the FEM using quadrilateral elements (FEM-Q4), the FEM using triangular elements (FEM-T3), and the N-SFEM using triangular elements (N-SFEM-T3). This example problem reveals the following facts: (1) the results of the αFEM-T3 in both the displacement and energy error norms at $\alpha_{exact} = 0.5635$ are much better than any of method, as shown in Figs. 9 and 10; (2) the FEM-Q4 is more accurate than either FEM-T3 or N-SFEM-T3, which justify why FEM-Q4 is much more widely used; (3) the αFEM-T3 gives much more accurate results than the popular FEM-Q4 in both norms. This finding is very important because we now can use triangular elements that can be generated automatically to obtain solutions that is far more accurate than quadrilateral elements that is difficult to generate automatically for complicated domains.

6.2. Cook's membrane: test for membrane elements in the skewed mesh

This benchmark problem, shown in Fig. 11, refers to a clamped tapered panel subjected to an in-plane shearing load, resulting in

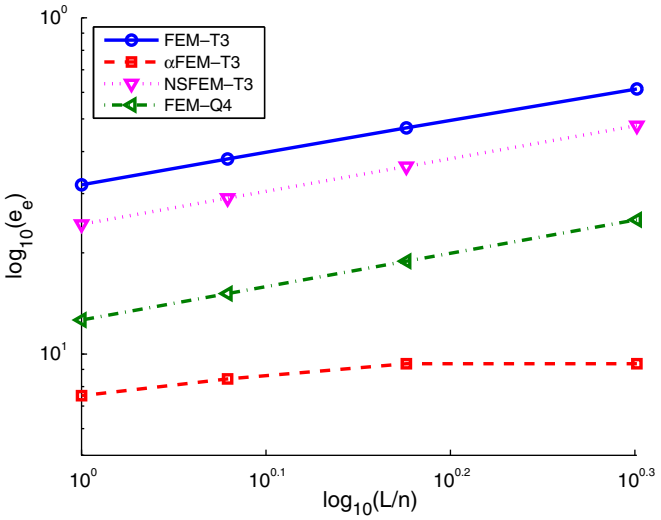

Fig. 9. Comparison of strain energy error norm of methods.

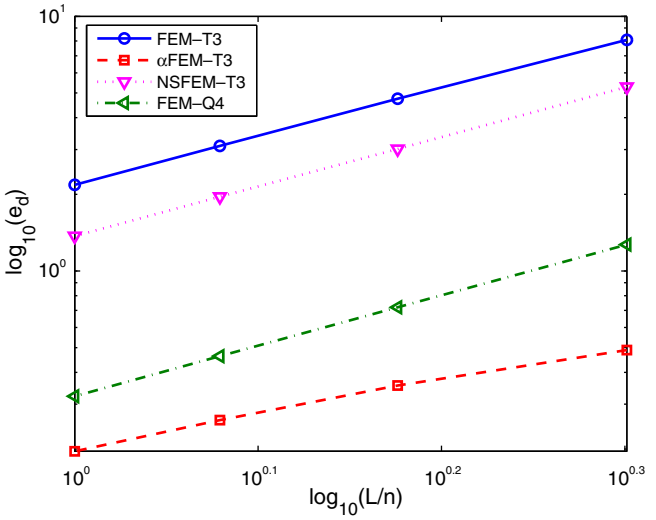

Fig. 10. Comparison of displacement error norm of methods.

deformation dominated by a bending response. This is a well known Cook's membrane problem [31] with Young's modulus $E = 1$, Poisson's ratio $\nu = 1/3$. The exact solution of the problem is unknown. Under plane stress conditions, the reference value of the vertical displacement at center tip section is 23.9642 [32] and the reference value of the strain energy is 12.015 [31]. Use the αFEM-T3, from Fig. 12, the estimated solutions at $\alpha_{exact} = 0.5085$ are 23.9748 for displacement tip and 12.0242 for strain energy.

Fig. 13 compare the result of displacement tip of the αFEM-T3 with six published four-node quadrilateral elements: Q4-standard isoparametric 2×2 quadrature Gauss points, Qm6-modified Wilson element [33], FB-one Gauss point with hourglass stabilization [34], QBI-Quintessential bending/incompressible element [35], KF-one Gauss point with hourglass control [36] and Qnew – an improved stabilization technique for one-point quadrature integration method [32]. It can be seen that the result of the αFEM-T3 at $\alpha_{exact} = 0.5085$ is more accurate than those of all the other elements, even with coarse meshes.

In addition to the results shown in Fig. 13, we make comparison of the αFEM-T3 with other elements for coarse meshes, and the results in numbers are listed in Table 4: Allman's membrane triangle

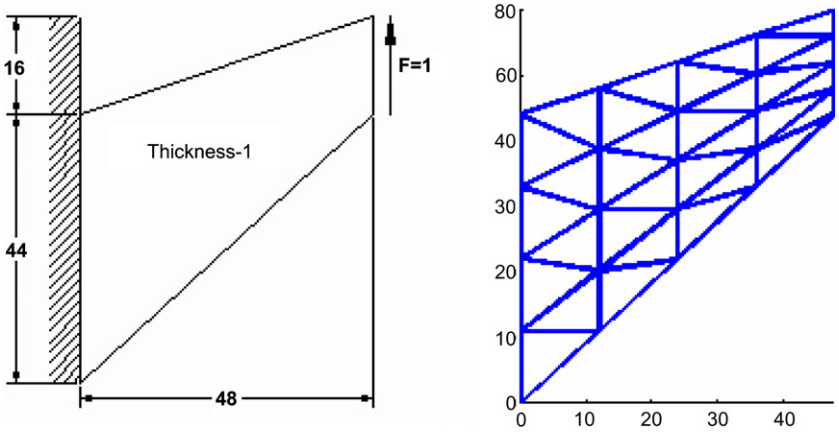

Fig. 11. Cook's membrane problem and its dicretization.

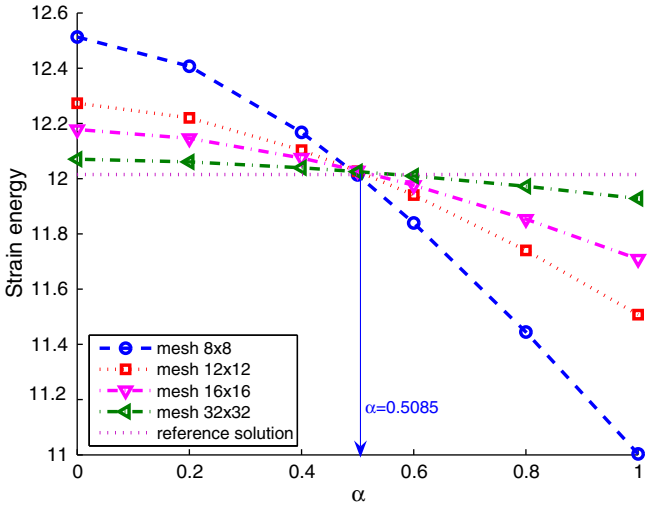

Fig. 12. Strain energy for Cook's membrane problem.

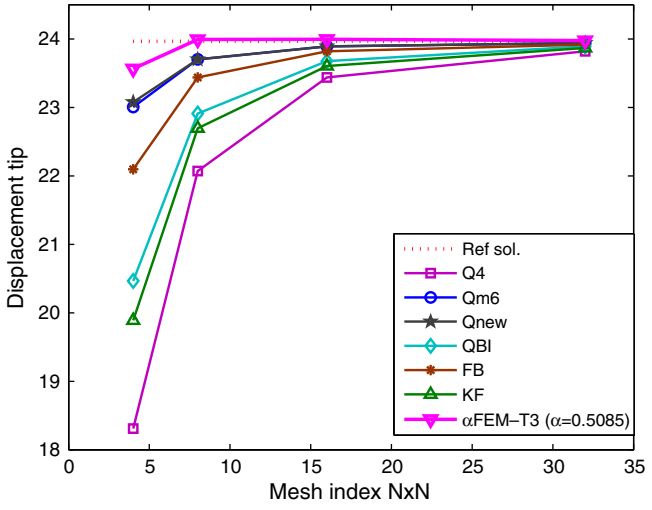

Fig. 13. Convergence of displacement tip for Cook's membrane.

(AT) [1], assumed stress hybrid methods such as Pian–Sumihara's element (P–S) [37], HQM/HQ4 element [38], Zhou–Nie's element (CH(0–1)) [39] and Xie–Zhou's element (ECQ4/LQ6) [40]. It is again found that the αFEM-T3 at $\alpha_{exact} = 0.5085$ gives the excellent performance compared to other elements.

Table 4
Results of displacement tip and strain energy for Cook's problem

	Displacement tip		Strain energy	
Elements	Mesh 4 × 4	Mesh 8 × 8	Mesh 4 × 4	Mesh 8 × 8
AT	22.41 (75)[a]	23.45 (243)	11.22	11.75
P–S	23.02 (50)	23.69 (162)	11.51	11.85
CH(0–1)	23.48 (50)	23.81 (162)	11.75	11.91
ECQ4/LQ6	23.48 (50)	23.81 (162)	11.75	11.91
HMQ/HQ4	23.04 (50)	23.69 (162)	11.52	11.85
α FEM-T3	23.56 (50)	23.99 (162)	11.77	12.00
Reference value	23.9642	23.9642	12.015	12.015

[a] Number of degrees of freedom denoted in parenthesis.

6.3. Infinite plate with a circular hole: test for volumetric locking

Fig. 14 represents a plate with a central circular hole of radius $a = 1$ m, subjected to a unidirectional tensile load of $\sigma = 1.0$ N/m at infinity in the x-direction. Due to its symmetry, only the upper right quadrant of the plate is modeled. Plane strain condition is considered and $E = 1.0 \times 10^3$ N/m^2, $\nu = 0.4/0.49/0.499/0.4999/0.49999/0.499999/0.4999999$. Symmetric conditions are imposed on the left and bottom edges, and the inner boundary of the hole is traction free. The exact solution for the stress is [30]

$$\begin{aligned}
\sigma_{11} &= 1 - \frac{a^2}{r^2}\left[\frac{3}{2}\cos 2\theta + \cos 4\theta\right] + \frac{3a^4}{2r^4}\cos 4\theta,\\
\sigma_{22} &= -\frac{a^2}{r^2}\left[\frac{1}{2}\cos 2\theta - \cos 4\theta\right] - \frac{3a^4}{2r^4}\cos 4\theta,\\
\tau_{12} &= -\frac{a^2}{r^2}\left[\frac{1}{2}\sin 2\theta + \sin 4\theta\right] + \frac{3a^4}{2r^4}\sin 4\theta,
\end{aligned} \tag{57}$$

where (r,θ) are the polar coordinates and θ is measured counter-clockwise from the positive x-axis. Traction boundary conditions are imposed on the right ($x = 5.0$) and top ($y = 5.0$) edges based on the exact solution Eq. (57). The displacement components corresponding to the stresses are

$$\begin{aligned}
u_1 &= \frac{a}{8\mu}\left[\frac{r}{a}(\kappa+1)\cos\theta + 2\frac{a}{r}((1+\kappa)\cos\theta + \cos 3\theta) - 2\frac{a^3}{r^3}\cos 3\theta\right],\\
u_2 &= \frac{a}{8\mu}\left[\frac{r}{a}(\kappa-1)\sin\theta + 2\frac{a}{r}((1-\kappa)\sin\theta + \sin 3\theta) - 2\frac{a^3}{r^3}\sin 3\theta\right],
\end{aligned} \tag{58}$$

where $\mu = E/(2(1+\nu))$, κ is defined in terms of Poisson's ratio by $\kappa = 3 - 4\nu$ for plane strain cases.

For the plane strain problem in the nearly incompressible case, $\alpha = 0$ and $\alpha = 0.5 - \nu$ as presented in Section 4.2 will be used in the

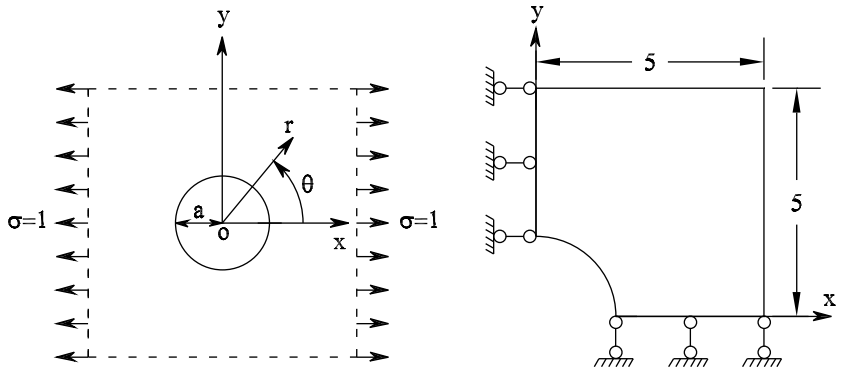

Fig. 14. Infinite plate with a circular hole and its quarter model.

Table 5
Displacement error norm (%) vs. different Poisson's ratios

Mesh	Poisson's ratios	αFEM-T3 $\alpha = 0$	αFEM-T3 $\alpha = 0.5 - \nu$	FEM-T3	FEM-Q4
12 × 12	$\nu = 0.4$	1.6937		1.7520	0.5633
12 × 12	$\nu = 0.49$	1.6222	1.5957	4.9955	2.9279
12 × 12	$\nu = 0.499$	1.6188	1.6148	7.7692	9.6562
12 × 12	$\nu = 0.4999$	1.6192	1.6188	8.3926	15.7707
12 × 12	$\nu = 0.49999$	1.6193	1.6192	8.4680	17.1450
12 × 12	$\nu = 0.499999$	1.6193	1.6192	8.4759	17.3087
12 × 12	$\nu = 0.4999999$	1.6193	1.6192	8.4767	17.3253

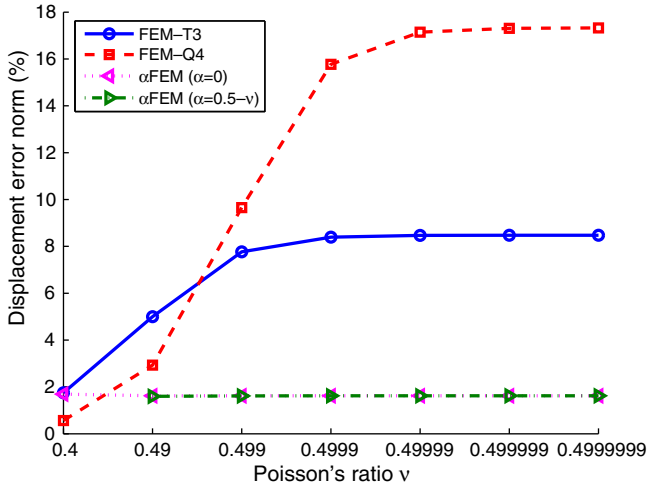

Fig. 15. Displacement error norm vs. different Poisson's ratios.

αFEM-T3. Table 5 and Fig. 15 show the displacement error norm vs. different Poisson's ratios for the αFEM-T3, FEM-T3 and the FEM-Q4 (mesh 12 × 12). The results show that the αFEM-T3 avoids the volumetric locking naturally, while the FEM-T3 and FEM-Q4 are clearly suffered from the volumetric locking. The results of the αFEM-T3 using $\alpha = 0.5 - \nu$ are little better than those simply using $\alpha = 0$, and hence are recommended by this paper. Note also that using $\alpha = 0.5 - \nu$ can also help to stabilize the solution for dynamic problems.

6.4. A cantilever beam subjected to a tip load: a large deformation analysis

The use of αFEM for large deformation analysis of a cantilever beam subjected to a concentrated tip load is now examined in this

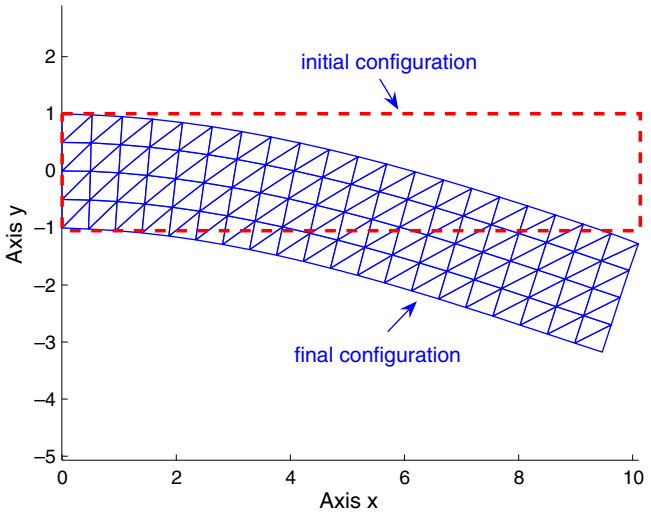

Fig. 16. The initial and final configuration of a 2D cantilever beam subjected to a tip load.

example. The size of the beam is (10 cm × 2 cm) and initially discretized using mesh 20 × 4. The related parameters are taken as $E = 3.0 \times 10^7$ kPa, $\nu = 0.3$. The analysis based on the total Lagrange formulation under the plane strain condition is carried out using 20 increment steps ($n = 20$) with $\Delta F = 10$ KN in each step.

Fig. 16 plots the initial and final configuration after 20 steps of increment of the deformation using the αFEM-T3 with $\alpha = 0.6$. Table 6 and Fig. 17 show the relation between the tip deflection vs. the load step. The simulation converges in a very rapid speed and in each load increment the iteration is performed less than 5 times. It can be seen that, with the same nodes, the FEM-T3 behaves much stiffer than the FEM-Q4. The results show that the nonlinear effect makes the cantilever beam behave much stiffer when compared to the linear solutions with the increase of loading. The results of the FEM-Q4 is bounded by those of αFEM-T3 using $\alpha = 0.5$ and $\alpha = 0.7$ in a very small range. When $\alpha = 0.6$ is used, the αFEM-T3 is quite close to the FEM-Q4. This shows that the αFEM-T3 with $\alpha \in \overline{0.5 : 0.7}$ works well in the 2D nonlinear analysis compared to solution of the FEM-Q4.

6.5. A 3D cubic cantilever: accuracy study

Consider a 3D cantilever of cubic shape, submitted to a uniform pressure on its upper face as shown in Fig. 18. The exact solution of the problem is unknown. By incorporating the solutions of hexahedral super-element elements and the procedure of Richardson's

Table 6
Tip deflection (cm) vs. the load step

Load step	FEM-T3 (linear)	FEM-T3 (nonlinear)	FEM-Q4 (linear)	FEM-Q4 (nonlinear)	αFEM-T3 (α = 0.5) (nonlinear)	αFEM-T3 (α = 0.6) (nonlinear)	αFEM-T3 (α = 0.7) (nonlinear)
$n = 2$	0.2518	0.2440 (3)[a]	0.2989	0.2841 (3)	0.2972 (3)	0.2879 (3)	0.2776 (3)
$n = 4$	0.5037	0.4569 (3)	0.5977	0.5225 (3)	0.5440 (3)	0.5286 (3)	0.5118 (3)
$n = 6$	0.7555	0.6467 (3)	0.8966	0.7387 (3)	0.7699 (3)	0.7475 (3)	0.7234 (3)
$n = 8$	1.0074	0.8272 (3)	1.1955	0.9541 (4)	0.9953 (4)	0.9657 (4)	0.9341 (4)
$n = 10$	1.2592	1.0101 (4)	1.4943	1.1614 (4)	1.2136 (4)	1.1761 (4)	1.1360 (4)
$n = 12$	1.5111	1.1847 (4)	1.7932	1.3684 (4)	1.4320 (4)	1.3864 (4)	1.3376 (4)
$n = 14$	1.7629	1.3589 (4)	2.0921	1.5754 (4)	1.6502 (4)	1.5966 (4)	1.5391 (4)
$n = 16$	2.0148	1.5330 (4)	2.3909	1.7821 (4)	1.8652 (5)	1.8047 (5)	1.7405 (4)
$n = 18$	2.2666	1.7069 (4)	2.6898	1.9844 (5)	2.0796 (5)	2.0114 (5)	1.9382 (5)
$n = 20$	2.5185	1.8795 (5)	2.9886	2.1872 (5)	2.2930 (5)	2.2173 (5)	2.1359 (5)

[a] The number in the bracket shows the number of iterations.

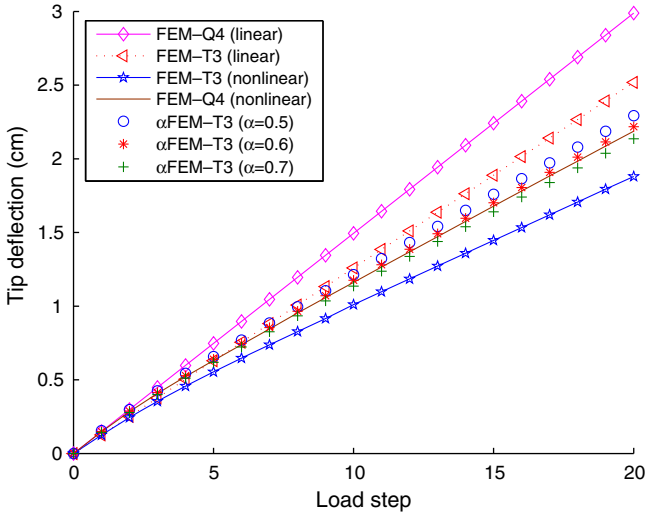

Fig. 17. Tip deflection (cm) vs. the load step.

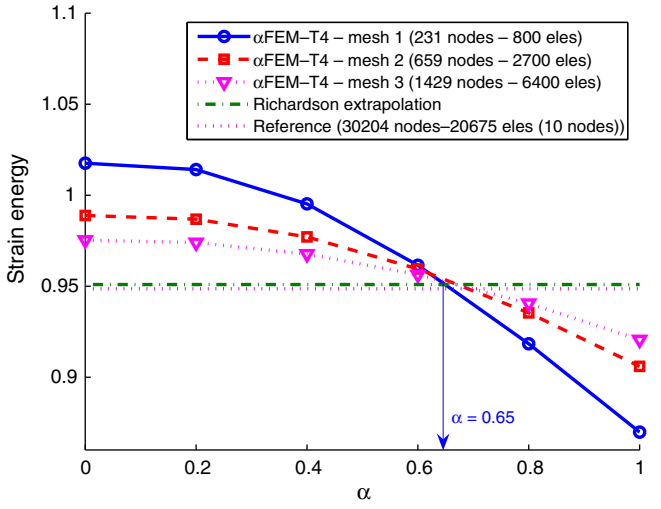

Fig. 19. Strain energy of the cubic cantilever.

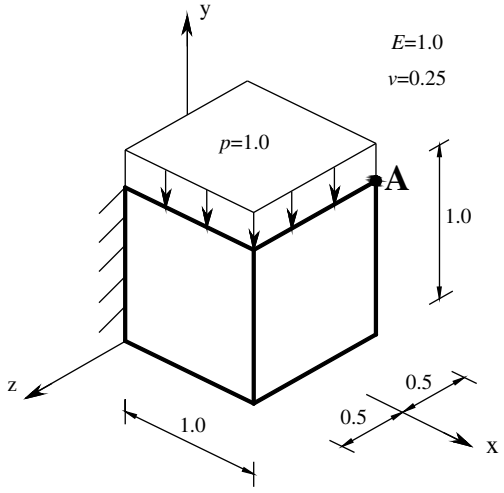

Fig. 18. A 3D cubic cantilever subjected to a uniform pressure on the top surface.

extrapolation, Almeida Pereira [41] gave an approximation of the exact strain energy to be 0.950930. From Fig. 19, the estimated strain energy obtained using αFEM-T4 is 0.95405 at $\alpha_{exact} = 0.65$. The difference between the estimated strain energy with the reference solution is as small as 0.33%. Using standard FEM and a very fine mesh with 30,204 nodes and 20,675 10-node tetrahedron elements, an other reference solution of the strain energy is found to be $E = 0.9486$. Comparing to this reference solution, the difference is also very small of 0.57%. Also from this reference, the deflection at point A (1.0, 1.0, −0.5) is 3.3912 and is compared with the results of the αFEM-T4 and FEM-T4 as shown in Table 7. It is shown that the αFEM-T4 at $\alpha_{exact} = 0.65$ gives the very good results even with coarse mesh, while the standard FEM-T4 behaves very stiff and converges much slower.

Table 7
Deflection at point A

	Mesh 1 (231 nodes)	Mesh 2 (659 nodes)	Mesh 3 (1429 nodes)	Reference solution
FEM-T4	3.1406	3.2595	3.3079	3.3912
αFEM-T4 ($\alpha_{exact} = 0.65$)	3.3981	3.4051	3.4012	3.3912

6.6. A 3D L-shaped block: accuracy study

Consider the 3D square block with a cubic hole subjected to the surface traction q as shown in Fig. 20. Due to the double symmetry of the problem, only a quarter of the domain is modeled, which becomes a 3D L-shaped block. The analysis is performed using input data: $q = 1, a = 1$, $E = 1, \nu = 0.3$. For this problem, the strain energy of 6.19985060 given by Cugnon [42] is considered as the reference solution. From Fig. 21, the estimated strain energy of the αFEM-T4 is 6.2057 at $\alpha_{exact} = 0.6873$. The difference between

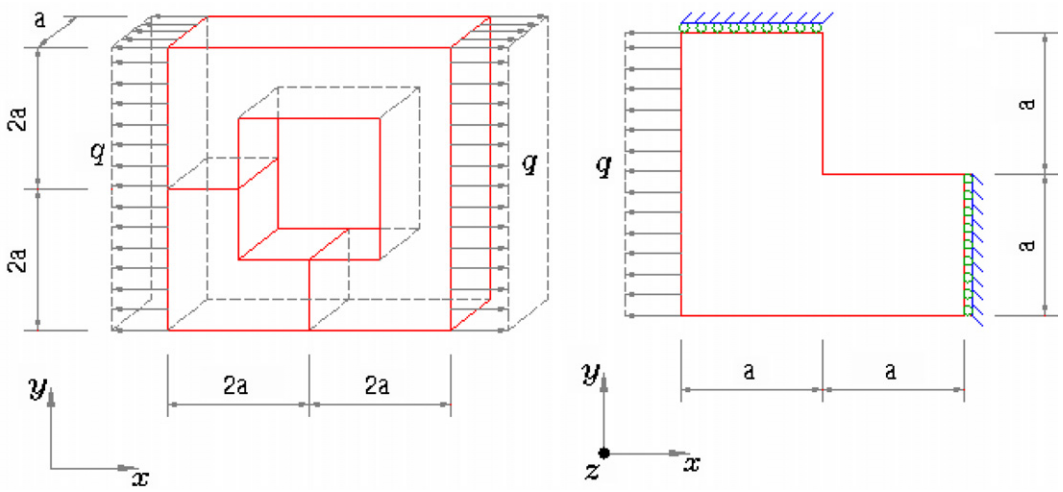

Fig. 20. 3D L-shaped problem and a quarter of the domain modeled.

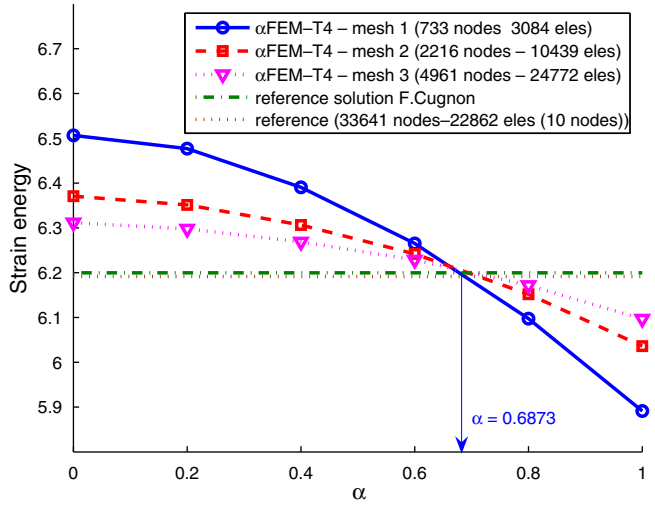

Fig. 21. Strain energy of the L-shaped 3D problem.

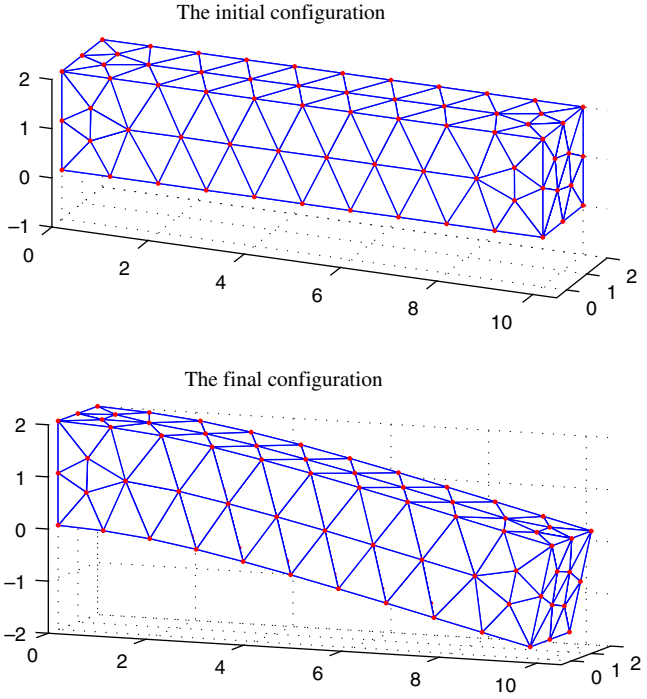

Fig. 22. The initial and final configuration of a 3D cantilever beam subjected to the regular distributed load using four-node tetrahedral elements.

the estimated strain energy with the reference solution is as small as 0.094%. Using standard FEM and a very fine mesh with 33,641 nodes and 22,862 10-node tetrahedron elements, an other reference solution of the strain energy is found to be $E = 6.1916$. Comparing to this reference solution, the difference is also very small of 0.23%.

6.7. A 3D cantilever beam subjected to a regular distributed load: a large deformation analysis

This example examines again the use of the αFEM for large deformation analysis for 3D solids. A 3D cantilever beam subjected to a regular distributed load is considered. The size of the beam is (10 cm × 2 cm× 2 cm) and discretized using a mesh including 117 nodes and 298 tetrahedral elements. The related parameters are taken as $E = 3.0 \times 10^7$ kPa, $\nu = 0.3$. The analysis based on the total Lagrange formulation is carried out using 20 increment steps ($n = 20$) with $\Delta f = 2$ KN/cm^2 in each step.

Fig. 22 displays the initial and final configuration after 20 steps of increment of the deformation using the αFEM-T4 with $\alpha = 0.7$. Table 8 and Fig. 23 show the relation between the tip deflection vs. the load step of different methods. The simulation converges in a very rapid speed and in each load increment, only less than five

Table 8
Tip deflection (m) vs. the load step

Load step	FEM-T4 (linear) (117 nodes)	FEM-T4 (nonlinear) (117 nodes)	FEM-H8 (nonlinear) (936 nodes)	αFEM-T4 ($\alpha = 0.7$) (nonlinear) (117 nodes)
$n = 2$	0.1838	0.1814 (3)[a]	0.2413 (3)	0.2505 (3)
$n = 4$	0.3675	0.3504 (3)	0.4509 (3)	0.4659 (3)
$n = 6$	0.5513	0.5040 (3)	0.6386 (3)	0.6593 (3)
$n = 8$	0.7351	0.6462 (3)	0.8180 (3)	0.8452 (3)
$n = 10$	0.9189	0.7819 (3)	0.9991 (4)	1.0325 (4)
$n = 12$	1.1026	0.9141 (3)	1.1726 (4)	1.2128 (4)
$n = 14$	1.2864	1.0516 (4)	1.3452 (4)	1.3925 (4)
$n = 16$	1.4702	1.1797 (4)	1.5173 (4)	1.5717 (4)
$n = 18$	1.6540	1.3070 (4)	1.6887 (4)	1.7502 (4)
$n = 20$	1.8377	1.4337 (4)	1.8594 (4)	1.9251 (5)

[a] The number in the bracket shows the number of iterations.

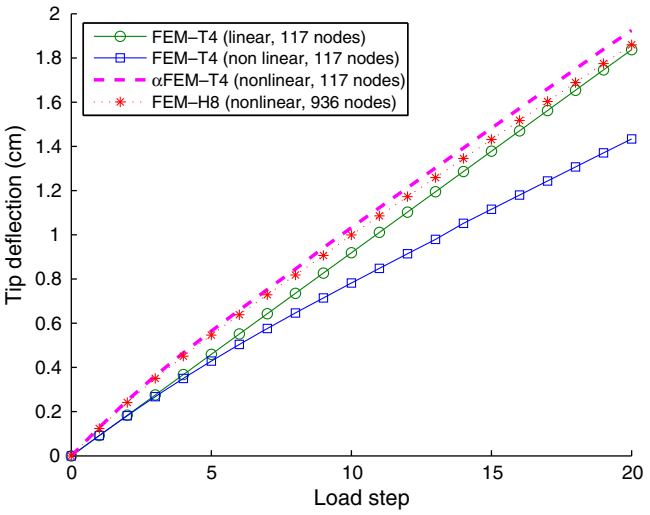

Fig. 23. Tip deflection (cm) vs. the load step.

times of iteration are performed. It can be seen that, the nonlinear effects make the cantilever beam behave stiffer compared to the linear solutions. In the nonlinear analysis, when $\alpha = 0.7$ is used, the results of αFEM-T4 is softer than those of FEM-T4 and is even very close to those of the FEM using eight-node hexahedral element (FEM-H8) using 936 nodes. This shows that the αFEM-T4 works very effectively for 3D nonlinear large deformation analysis.

7. Conclusion

In this work, a novel alpha finite element method with a scale factor α of three-node triangular (αFEM-T3) and four-node tetrahedral (αFEM-T4) elements is proposed. Through the theoretical study and numerical examples, the following major conclusions can be drawn:

- The αFEM-T3 and αFEM-T4 ensure the variational consistence and the compatibility of the displacement field, and hence they guarantee to reproduce linear field exactly for any $\alpha \in [0,1]$.
- The αFEM-T3 and αFEM-T4 are equipped with a scaling factor α that controls the contributions from the N-SFEM and the FEM. When the factor α varies from 0 to 1, a continuous solution function from the solution of the N-SFEM to that of the FEM is obtained. When $\alpha = 0$, the αFEM-T3 and αFEM-T4 becomes the N-SFEM, and the strain energy $E(\alpha = 0)$ is an upper bound of the exact strain energy. When $\alpha = 1$, the αFEM-T3 and αFEM-T4 becomes the standard FEM, and the strain energy $E(\alpha = 1)$ is a lower bound of the exact strain energy.
- From the observed behavior of the numerical results, a unique approach of the αFEM-T3 and αFEM-T4 has been proposed to obtain the nearly exact solution in strain energy for problems using meshes with the same aspect ratio. The corresponding displacement solution is also much better comparing those of the standard FEM and the N-SFEM. The αFEM-T3 and αFEM-T4 are capable to provide a "nearly exact" solution in strain energy with very coarse meshes.
- The implementation of αFEM-T3 (or αFEM-T4) in practical applications is very easy and quite similar to the standard FEM because of two reasons: (1) automatic refinement from an initial coarse mesh to obtain the meshes with the same aspect ratio is available in many automatic programs basing on creating three-node triangular and four-node tetrahedral elements; (2) the proposed methods use the strain matrices **B** of the standard FEM and area (or volume) of elements to calculate the system stiffness matrix. No new numerical integration is necessary.
- For the nearly incompressible cases of the plane strain problems, some values of α are recommended to solve the volumetric locking problem.
- The αFEM-T3 and αFEM-T4 can be used to improve the accuracy of the solutions of nonlinear problems of large deformation.
- The obtained result from this study is very promising and the αFEM-T3 (or αFEM-T4) can be applied easily into the available commercial software with little modification.
- The αFEM-T3 (or αFEM-T4) is suitable for adaptive analysis as it uses only triangular and tetrahedral elements that can be automatically generated for complicated domains.

References

[1] D.J. Allman, A compatible triangular element including vertex rotations for plane elasticity analysis, Comput. Struct. 19 (2) (1984) 1–8.
[2] D.J. Allman, Evaluation of the constant strain triangle with drilling rotations, Int. J. Numer. Method Engrg. 26 (12) (1988) 2645–2655.
[3] P.G. Bergan, C.A. Felippa, A triangular membrane element with rotational degrees of freedom, Comput. Method Appl. Mech. Engrg. 50 (1985) 25–69.
[4] R.D. Cook, Modified formulations for nine-dof plane triangles that include vertex rotations, Int. J. Numer. Method Engrg. 31 (1991) 825–835.
[5] R. Piltner, R.L. Taylor, Triangular finite elements with rotational degrees of freedom and enhanced strain modes, Comput. Struct. 75 (2000) 361–368.
[6] C.R. Dohrmann, S.W. Key, M.W. Heinstein, J. Jung, A least squares approach for uniform strain triangular and tetrahedral finite elements, Int. J. Numer. Method Engrg. 42 (1998) 1181–1197.
[7] C.R. Dohrmann, M.W. Heinstein, J. Jung, S.W. Key, W.R. Witkowski, Node-based uniform strain elements for three-node triangular and four-node tetrahedral meshes, Int. J. Numer. Method Engrg. 47 (2000) 1549–1568.
[8] J.S. Chen, C.T. Wu, S. Yoon, Y. You, A stabilized conforming nodal integration for Galerkin meshfree method, Int. J. Numer. Method Engrg. 50 (2000) 435–466.
[9] J.W. Yoo, B. Moran, J.S. Chen, Stabilized conforming nodal integration in the natural-element method, Int. J. Numer. Method Engrg. 60 (2004) 861–890.
[10] G.R. Liu, G.Y. Zhang, K.Y. Dai, Y.Y. Wang, Z.H. Zhong, G.Y. Li, X. Han, A linearly conforming point interpolation method (LC-PIM) for 2D solid mechanics problems, Int. J. Comput. Method 2 (4) (2005) 645–665.
[11] G.R. Liu, Y. Li, K.Y. Dai, M.T. Luan, W. Xue, A Linearly conforming radial point interpolation method for solid mechanics problems, Int. J. Comput. Method 3 (4) (2006) 401–428.
[12] G.R. Liu, T.T. Nguyen, K.Y. Dai, K.Y. Lam, Theoretical aspects of the smoothed finite element method (SFEM), Int. J. Numer. Method Engrg. 71 (2007) 902–930.
[13] K.Y. Dai, G.R. Liu, T.T. Nguyen, An *n*-sided polygonal smoothed finite element method (nSFEM) for solid mechanics, Finite Elem. Anal. Des. 43 (2007) 847–860.
[14] G.R. Liu, T.T. Nguyen, X.H. Nguyen, K.Y. Lam, A node-based smoothed finite element method for upper bound solution to solid problems (N-SFEM), Comput. Struct. (Revised).
[15] G.R. Liu, G.Y. Zhang, Upper bound solution to elasticity problems: A unique property of the linearly conforming point interpolation method (LC-PIM), Int. J. Numer. Method Engrg. in press (Published online 8 Oct, 2007).
[16] D.N. Arnold, Mixed finite element methods for elliptic problems, Comput. Method Appl. Mech. Engrg. 82 (1990) 281–300.
[17] T.Y. Rong, A.Q. Lu, Generalized mixed variational principles and solutions for ill-conditioned problems in computational mechanics: Part I. Volumetric locking, Comput. Method Appl. Mech. Engrg. 191 (2001) 407–422.
[18] T.Y. Rong, A.Q. Lu, Generalized mixed variational principles and solutions for ill-conditioned problems in computational mechanics: Part II. Shear locking, Comput. Method Appl. Mech. Engrg. 192 (2003) 4981–5000.
[19] D. Mijuca, M. Berković, On the efficiency of the primal-mixed finite element scheme, Advances in Computational Structured Mechanics, Civil-Comp Press, 1998. pp. 61–69.
[20] T.T. Nguyen, G.R. Liu, K.Y. Lam, A FEM using scaled gradient of strains with scaling factor alpha (alpha-FEM), in: Proceeding of the International Conference on Computational Methods 2007 (ICCM07), 2007, p. 194.
[21] G.R Liu, T.T. Nguyen, K.Y. Lam, A novel FEM by scaling the gradient of strains with scaling factor α (αFEM), Comput. Mech. (revised).
[22] KJ. Bathe, Finite Element Procedures, Prentice Hall, Massachusett (MIT), 1996.
[23] C. Johnson, Numerical Solution of Partial Differential Equations by the Finite Element Method, Cambridge University Press, New York, 1987.
[24] T.J.R. Hughes, The Finite Element Method: Linear Static and Dynamic Finite Element Analysis, Prentice-Hall, 1987.
[25] G.R. Liu, S.S. Quek, The Finite Element Method: A Practical Course, Butterworth Heinemann, Oxford, 2003.
[26] O.C. Zienkiewicz, R.L. Taylor, The Finite Element Method, fifth ed., Butterworth Heinemann, Oxford, 2000.
[27] J.N. Reddy, An Introduction to Nonlinear Finite Element Analysis, Oxford University Press, 2004.

[28] T.H.H. Pian, C.C. Wu, Hybrid and Incompatible Finite Element Methods, CRC Press, Boca Raton, 2006.
[29] J.C. Simo, T.J.R. Hughes, On the variational foundations of assumed strain methods, J. Appl. Mech. 53 (1986) 51–54.
[30] S.P. Timoshenko, J.N. Goodier, Theory of Elasticity, third ed., McGraw-Hill, New York, 1970.
[31] R. Cook, Improved two-dimensional finite element, J. Struct. Div., ASCE 100 (ST6) (1974) 1851–1863.
[32] M. Fredriksson, N.S. Ottosen, Fast and accurate four-node quadrilateral, Int. J. Numer. Method Engrg. 61 (2004) 1809–1834.
[33] R.L. Taylor, P.J. Beresford, E.L. Wilson, A non-conforming element for stress analysis, Int. J. Numer. Method Engrg. 10 (1976) 1211–1219.
[34] D.P. Flanagan, T. Belytschko, A uniform strain hexahedron and quadrilateral with orthogonal hourglass control, Int. J. Numer. Method Engrg. 17 (1981) 679–706.
[35] T. Belytschko, E. Bachrach, Efficient implementation of quadrilaterals with high coarse-mesh accuracy, Comput. Method Appl. Mech. Engrg. 54 (1986) 279–301.
[36] D. Kosloff, G.A. Frazier, Treatment of hourglass patterns in low order finite element codes, Int. J. Numer. Anal. Method Geomech. 2 (1978) 57–72.
[37] T.H.H. Pian, K. Sumihara, Rational approach for assumed stress finite elements, Int. J. Numer. Method Engrg. 20 (1984) 1685–1695.
[38] X. Xie, An accurate hybrid macro-element with linear displacements, Commun. Numer. Method Engrg. 21 (2005) 1–12.
[39] T. Zhou, Y. Nie, A combined hybrid approach to finite element schemes of high performance, Int. J. Numer. Method Engrg. 51 (2001) 181–202.
[40] X. Xie, T. Zhou, Optimization of stress modes by energy compatibility for four-node hybrid quadrilaterals, Int. J. Numer. Method Engrg. 59 (2004) 293–313.
[41] O.J.B. Almeida Pereira, Hybrid equilibrium hexahedral elements and super-elements, Commun. Numer. Method Engrg. 24 (2) (2008) 157–165.
[42] F. Cugnon, Automatisation des calculs elements finis dans le cadre de la methode-p, Universite de Lie, Ph.D. Thesis, 2000.
[43] G.R. Liu, K.Y. Dai, T.T. Nguyen, A smoothed finite element method for mechanics problems, Comput. Mech. 39 (2007) 859–877.